Mon. Not. R. Astron. Soc. **000**, 000–000 (0000) Printed 17 June 2011 (MN LaTeX style file v2.2)

The life cycle of star clusters in a tidal field

Mark Gieles[1], Douglas C. Heggie[2], HongSheng Zhao[3]
[1] *Institute of Astronomy, University of Cambridge, Madingley Road, Cambridge, CB3 0HA, UK*
[2] *School of Mathematics and Maxwell Institute for Mathematical Sciences, University of Edinburgh, Kings Buildings, Edinburgh EH9 3JZ*
[3] *Scottish University Physics Alliance, University of St. Andrews, KY16 9SS, UK*

Accepted 2011 January 9. Received 2011 January 9; in original form 2010 November 22

ABSTRACT

The evolution of globular clusters due to 2-body relaxation results in an outward flow of energy and at some stage all clusters need a central energy source to sustain their evolution. Hénon provided the insight that we do not need to know the details of the energy production in order to understand the relaxation-driven evolution of the cluster, at least outside the core. He provided two self-similar solutions for the evolution of clusters based on the view that the cluster as a whole determines the amount of energy that is produced in the core: steady expansion for isolated clusters, and homologous contraction for clusters evaporating in a tidal field. The amount of expansion or evaporation per relaxation time-scale is set by the instantaneous radius or number of stars, respectively. We combine these two approximate models and propose a pair of Unified Equations of Evolution (UEE) for the life cycle of initially compact clusters in a tidal field. The half-mass radius increases during the first part (roughly half) of the evolution, and decreases in the second half; while the escape rate approaches a constant value set by the tidal field. We refer to these phases as 'expansion dominated' and 'evaporation dominated'. These simple analytical solutions of the UEE immediately allow us to construct evolutionary tracks and isochrones in terms of cluster half-mass density, cluster mass and galacto-centric radius. From a comparison to the Milky Way globular clusters we find that roughly one-third of them are in the second, evaporation-dominated phase and for these clusters the density inside the half-mass radius varies with the galactocentric distance $R_{\rm G}$ as $\rho_{\rm h} \propto R_{\rm G}^{-2}$. The remaining two-thirds are still in the first, expansion-dominated phase and their isochrones follow the environment-independent scaling $\rho_{\rm h} \propto M^2$, where M is the cluster mass; that is, a constant relaxation time-scale. We find substantial agreement between Milky Way globular cluster parameters and the isochrones, which suggests that there is, as Hénon suggested, a balance between the flow of energy and the central energy production for almost all globular clusters.

Key words: galaxies: star clusters – globular clusters: general

1 INTRODUCTION

Globular clusters strive their entire life for thermal equilibrium, but their negative heat capacity prevents them from ever reaching this. As a result there is a continuous flow of energy that is conducted outwards by relaxation. Any equations attempting to capture cluster evolution could be very complex and non-linear with many variables to keep track of since the dynamical evolution of star clusters is the result of several processes, including two-body relaxation, interactions with binary stars, escape across the tidal boundary, and the internal evolution and mass-loss of single and binary stars. Fig.1 illustrates typical results, in terms of the evolution of the core radius, the half-mass radius and the tidal radius. Within the first few times 10 Myr there is a rapid phase of mass segregation, leading to contraction of the core. (Note the logarithmic time scale in the figure.) At the end of this phase the half-mass radius starts to increase, and the expansion continues, but decelerates, over the next 8 Gyr approximately. At the same time the cluster is losing mass, both by the escape of stars and by the effects of stellar evolution, and this causes a decrease in the tidal radius. For the remaining evolution (up to 12 Gyr) the half-mass radius also contracts. Except for the initial phase of mass segregation, the core radius remains small compared with the half-mass radius; it also begins its contraction at about 6 Gyr, i.e. earlier than the half-mass radius, and subsequently drops to and fluctuates around a lower value.

Our theoretical aim in this paper is to provide a physically motivated and simple prescription for the behaviour of the half-mass and tidal radii in the period following the end of the phase of mass segregation, i.e. all except about the first 1% of the evolution of the cluster. With this we are able to construct evolutionary tracks and isochrones for clusters evolving in a tidal field and provide a theoretical framework for empirically established correlations between structural parameters and their environment as found for Milky Way globular clusters (e.g. Djorgovski 1995; McLaughlin 2000)

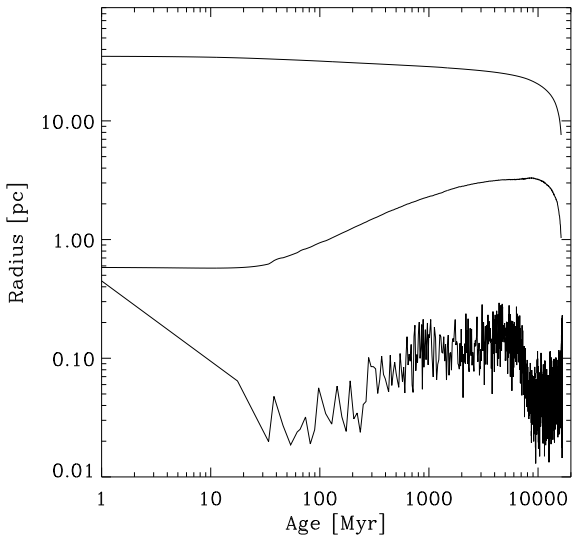

Figure 1. The evolution of the tidal, half-mass and core-radii (from top to bottom) in the evolution of a Monte Carlo model of the globular cluster M4 (from Heggie & Giersz 2008).

and for extra-galactic globular cluster systems (e.g. Jordán et al. 2005; Barmby et al. 2007; McLaughlin et al. 2008; Harris et al. 2010). We do not aim to explain the shape and dependence on environment of the globular cluster mass function at this stage, however. The other principal exclusion is that we do not attempt to model the evolution of the core. The fact that this programme will succeed is due to a number of important discoveries by Hénon.

The first of these discoveries (Hénon 1961) was a simple model of an idealised star cluster evolving in a tidal field. The main idealisations were that all stars have the same mass and do not evolve internally, the tidal field is modelled as a cutoff at the tidal radius, the system is non-rotating and spherically symmetric, there is no significant binary population, the velocity distribution of the stars at a point is isotropic, and gravitational encounters are modelled as a Fokker-Planck equation. Then Hénon showed that the system could evolve at constant mean density, with stars escaping across the tidal boundary, and the structure of the cluster at any time is simply a scaled version of the structure at any other time, i.e. the evolution is 'self-similar'. In particular, this means that the half-mass radius is a constant fraction of the tidal radius. We shall adapt this model to describe the evolution at late times in models such as that shown in Fig.1.

Hénon's next advance in this field (Hénon 1965) was the discovery of a similar model for an isolated system, i.e. one with no tide. It is again self-similar, but the total mass remains constant, and the half-mass radius increases. This we shall adapt to describe the evolution of models such as that shown in Fig.1, from the end of the phase of mass segregation until the point where the tidal radius begins to have a significant effect on the expansion of the half-mass radius. A further part of our adaptation will be to construct a way of bridging the transition between the two models, and to do so in a physically well motivated way.

The third discovery of Hénon explains why this programme can work even without detailed modelling of the core. In both of Hénon's models the energy of the system increases, and Hénon himself considered that the formation and hardening of binaries in the core was a plausible source of this energy[1]. It might have been thought, therefore, that the evolution of the system would depend on details of this source of energy and the radius and density of the core. But a correct understanding of the connection between the core and the evolution of the system as a whole came from the insight of Hénon (1975). He realised that the *rate of flow of energy is controlled by the system as a whole, and not by the core.* That is, it is not the cluster that responds to whatever happens in the core, but the other way around.

In Hénon's picture the mechanism of energy generation is self-regulatory, as is the case in stellar interiors, where the luminosity of the star is determined by how much radiation can be transported through the envelope. The nuclear fusion rate in the core of the star adjusts to it. The application of this idea to stellar dynamics was a breakthrough allowing modellers to overcome the core collapse phase. In the Monte Carlo models of Hénon (1975) the energy source is entirely artificial and unspecified. Later, it was found from N-body simulations of the long term (post-collapse) evolution of equal mass clusters that hard binaries act as the energy source (Giersz & Heggie 1994; Baumgardt et al. 2002). In more realistic N-body simulations of star clusters these binaries are usually considered to be primordial, but other mechanisms of energy generation have been modelled, including the action of a central intermediate-mass black hole (Baumgardt et al. 2004) and, less controversially, mass-loss from stellar evolution. Gieles et al. (2010) showed that mass loss as a consequence of stellar evolution also leads to a self-regulatory energy production, which works together with hard binaries in driving the long term evolution. Indeed, it may even dominate, as in the specific example of 47 Tuc (Giersz & Heggie 2011), a high-concentration cluster in which the evolution of the core- and half-mass radii appears to be little affected by the primordial binary population.

These self-regulatory mechanisms of energy generation take time to establish the balance between the energy generated in the core and the energy requirements of the overall evolution of the cluster. In Fig.1 this balance is reached at about the end of the phase of mass segregation. Mass segregation ceases close to the time when the core radius reaches a minimum for the first time. This was found from numerical simulations of clusters with a moderately wide mass spectrum (Giersz & Heggie 1996) and for clusters with a full mass spectrum (Portegies Zwart et al. 2007). The reason for this is not that equipartition has been reached, due to Spitzer's instability (Spitzer 1969). The origin of this quasi steady-state distribution of stars of different masses is not well understood theoretically, but it is taken as a given here. We refer to the subsequent evolution as 'balanced'. In much research on cluster dynamics this kind of evolution is usually associated with 'post-collapse' evolution, but this term is ambiguous; in Fig.1, for instance, the phrase 'post-collapse' might be used for the entire evolution after the end of mass segregation, but others might apply it to the evolution following the late decrease in the core radius in the last few Gyr. For this reason we prefer the term 'balanced evolution'.

Gieles et al. (2010) showed that the evolution of most globular clusters is balanced. Their result was based, however, on a comparison of the behaviour of clusters expanding in isolation to the structural parameters of relatively massive globular clusters ($\gtrsim$few$\times 10^4$ M$_\odot$) and ultra-compact dwarf galaxies. It was assumed implicitly that these are little affected by the tide. In the

[1] In fact Hénon (1961) introduces the concept of energy generation by the core in the other way around: the core absorbs negative energy.

present study we add the effect of a tidal field, which slows down the expansion of all clusters at some point in their evolution.

In Section 2 we discuss how the behaviour of the Hénon models in isolation and in tidal fields can be related to the flow of energy, and we show how the two extremes, expansion without mass loss and homologous contraction in a tidal field, may be unified. Isochrones in physical units at an age of a Hubble time are extracted and are compared to the data of Milky Way globular clusters in Section 3. A summary and discussion are presented in Section 4. The specific symbols used in this study are summarised in Table 1 and details of the derivations are presented in Appendices.

2 A UNIFIED MODEL OF EXPANSION AND EVAPORATION

2.1 The flux of energy

Our attempt to unify the evolution of mass and radius of the two models of Hénon begins with one of the physical properties which the two models have in common, i.e. a flux of energy at the half-mass radius which is fed by an energy source in the core. We constrain ourselves to the energy flow at this radius, because we can then construct a relatively simple set of relations for the behaviour of the bulk properties of the cluster. A full unification of the two models of Hénon requires numerically solving the Fokker-Planck equations (e.g. Cohn 1979, and follow-up studies). This would be needed to get the distribution function of energies and the density profile as a function of time, which is not the aim of this paper. For the present we adopt Hénon's idealisation of systems in which all stars have the same mass m. Then we estimate the energy as usual by

$$E = -\alpha \frac{GN^2m^2}{r_{\rm h}}, \tag{1}$$

where N is the number of stars, $r_{\rm h}$ is the half-mass radius, and α is a 'form factor' for which the value 0.2 is often taken (Spitzer 1987, p.12).

In Hénon's isolated model (Hénon 1965), all quantities on the right-hand side of equation (1) are constant except $r_{\rm h}$, and it follows from Hénon's equations (3), (6) and (7) that

$$\frac{\dot{E}}{|E|} = \frac{\dot{r}_{\rm h}}{r_{\rm h}} \simeq \frac{0.0926}{\tau_{\rm rh}}, \tag{2}$$

except that one also requires the value for the dimensionless half-mass radius $\mathbf{R}$, which is given in Hénon's paper on p.64. Also, we have expressed the result in terms of the conventional half-mass relaxation time (Spitzer 1987), i.e.

$$\tau_{\rm rh} = 0.138 \frac{N^{1/2} r_{\rm h}^{3/2}}{\sqrt{\bar{m}G}\ln\Lambda}, \tag{3}$$

where $\bar{m}$ is the mean stellar mass (i.e. m in this case) and $\ln\Lambda$ is the Coulomb logarithm, which we have equated with the factor Log n in Hénon's equation (7).

For Hénon's tidally limited model (Hénon 1961), both N and $r_{\rm h}$ vary because the cluster loses stars at a constant density, and a similar calculation leads to the result that

$$\frac{\dot{E}}{|E|} = -2\frac{\dot{N}}{N} + \frac{\dot{r}_{\rm h}}{r_{\rm h}} \simeq \frac{0.0743}{\tau_{\rm rh}}. \tag{4}$$

What is noticeable about equations (2) and (4) is how similar the final numerical coefficients are. Indeed, in constructing a unified approximate model which includes the transition from nearly isolated evolution to tidally limited evolution, we shall make the *assumption* that the numerical coefficient is constant, i.e. that

$$\frac{\dot{E}}{|E|} = \frac{\zeta}{\tau_{\rm rh}}, \tag{5}$$

where $\zeta \simeq 0.08$ in the case of equal masses. The accuracy of this approximation is comparable with the common approximation of treating α in equation (1) as constant.

Before proceeding further, we shall change one of the variables in which the total energy E is expressed, because this will facilitate one particular step in the further development of our model. Instead of using the half-mass radius, $r_{\rm h}$, we shall use the (half-mass) crossing time of the system, defined here as

$$\tau_{\rm cr} \equiv (G\rho_{\rm h})^{-1/2}, \tag{6}$$

with $\rho_{\rm h} \equiv 3M/(8\pi r_{\rm h}^3)$, the cluster density within the half-mass radius, and $M \equiv mN$ the total cluster mass. (Note that this differs from the conventional crossing time by a numerical factor; see also Table 1.) Putting this together with our assumption about the energy flux, we replace equations (2) and (4) by [2]

$$\frac{\dot{E}}{|E|} = \frac{\zeta}{\tau_{\rm rh}} = -\frac{5}{3}\frac{\dot{N}}{N} + \frac{2}{3}\frac{\dot{\tau}_{\rm cr}}{\tau_{\rm cr}}. \tag{7}$$

The constants become obvious when we look at the expression for the total energy (equation 1) in terms of N and $\tau_{\rm cr}$ (equation 6): $|E| \propto (mN)^{5/3}/\tau_{\rm cr}^{2/3}$. In the next subsection the relative contributions of expansion and evaporation to the energy flow are specified.

2.2 The relative importance of expansion and evaporation

Now we have a functional form that relates evaporation and expansion to the flow of energy (equation 7) we need to specify what the relative importance is of these two processes. The equations that follow (equaions 8–12) form the base for our analysis. We introduce two new coefficients, ξ and χ, to quantify the (dimensionless) evaporation rate and the (dimensionless) expansion rate, respectively.

$$\xi \equiv -\frac{\dot{N}\tau_{\rm rh}}{N}, \tag{8}$$

and

$$\chi \equiv \frac{\dot{\tau}_{\rm cr}\tau_{\rm rh}}{\tau_{\rm cr}}, \tag{9}$$

so that (see equation 7)

$$\zeta = \frac{2}{3}\chi + \frac{5}{3}\xi. \tag{10}$$

For Hénon's isolated model, $\xi = 0$, while $\chi = 0$ for the tidally bound model.

To get a full description of the behaviour of the mass and half-mass radius of the cluster we need to relate one of the coefficients ξ or χ to $\tau_{\rm cr}$ and N. Here we focus on the dimensionless escape-rate ξ. By estimating the fraction of stars above the escape velocity for tidally limited clusters with different ratios $r_{\rm h}/r_{\rm J}$, where $r_{\rm J}$ is the Jacobi (tidal) radius of the cluster, Lee (2002) and Gieles & Baumgardt (2008) have shown that $\ln\xi \propto r_{\rm h}/r_{\rm J}$, approximately. In principle we could proceed with this exponential function for ξ, but a more convenient approximation will make

[2] For clusters with a stellar mass spectrum there will be an additional term $-(5/3)(\dot{\bar{m}}/\bar{m})$ on the right-hand side.

Table 1. Overview of the specific symbols used in this study. The symbols with the subscript 1 are used to refer to the maximum value the variable can have.

Symbol	Definition	Description
$\rho_{\rm h}$	$3M/(8\pi r_{\rm h}^3)$	Mean density within the half-mass radius
$\rho_{\rm J}$	$3M/(4\pi r_{\rm J}^3)$	Mean density within the Jacobi radius
$(r_{\rm h}/r_{\rm J})_1$		Maximum ratio of the half-mass radius over the Jacobi radius
$\tau_{\rm cr}$	$(G\rho_{\rm h})^{-1/2}$	A measure of the crossing time at the half-mass radius
$\tau_{\rm cr}^{\rm J}$	$(G\rho_{\rm J})^{-1/2}$	Crossing time at the Jacobi radius
$\tau_{\rm cr1}$	$\sqrt{2}(r_{\rm h}/r_{\rm J})_1^{3/2}\tau_{\rm cr}^{\rm J}$	Crossing time at the half-mass radius for a homologous cluster, equation (16)
$\tau_{\rm rh}$	$CN\tau_{\rm cr}$	Approximate half-mass relaxation time, with $C \simeq 0.006$ (equations 13 & 14)
$\tau_{\rm ev0}$	see equation (23)	Total life-time of a cluster of N_0 stars
$\tau_{\rm ev}$	see equation (23)	Remaining life-time, or 'life-expectancy', of a clusters of N stars
ζ	$(\dot{E}/\lvert E\rvert)\tau_{\rm rh}$	Fraction of the total energy conducted per $\tau_{\rm rh}$
χ	$(\dot{\tau}_{\rm cr}/\tau_{\rm cr})\tau_{\rm rh}$	Dimensionless expansion rate
ξ	$-(\dot{N}/N)\tau_{\rm rh}$	Dimensionless escape rate

what is to follow much easier. In fact, Gieles & Baumgardt (2008) show that $\xi \propto (r_{\rm h}/r_{\rm J})^{3/2}$ provides a satisfactory approximation to the exponential function (in the relevant range of $r_{\rm h}/r_{\rm J}$). This relation can be expressed equivalently as $\xi \propto \tau_{\rm cr}$. As a cluster expands, $\tau_{\rm cr}$ increases, until the point where the cluster evolution becomes tidally limited, i.e. the point where its evolution begins to be analogous to the model of Hénon (1961). Let $\tau_{\rm cr1}$ denote the value of $\tau_{\rm cr}$ during this part of the evolution. Since $\tau_{\rm cr}$ is now constant, $\chi = 0$ (by equation 9), and so equation (10) implies that $\xi = (3/5)\zeta$ when $\tau_{\rm cr} = \tau_{\rm cr1}$. Putting these results together with equation (10), we arrive at a pair of Unified Equations of Evolution (UEE)

$$\xi \equiv -\frac{\dot{N}\tau_{\rm rh}}{N} = \frac{3}{5}\zeta\frac{\tau_{\rm cr}}{\tau_{\rm cr1}}, \quad (11)$$

$$\chi \equiv \frac{\dot{\tau}_{\rm cr}\tau_{\rm rh}}{\tau_{\rm cr}} = \frac{3}{2}\zeta\left(1-\frac{\tau_{\rm cr}}{\tau_{\rm cr1}}\right), \quad (12)$$

which we adopt henceforth. These two expressions for ξ and χ capture the behaviour of clusters for all values $0 \leqslant \tau_{\rm cr} \leqslant \tau_{\rm cr1}$. For $\tau_{\rm cr} \ll \tau_{\rm cr1}$ they give the desired self-similar expansion ($\chi \simeq (3/2)\zeta =$ constant and $\xi \simeq 0$) and the growth of $\tau_{\rm cr}$ stops when $\tau_{\rm cr} = \tau_{\rm cr1}$ ($\chi = 0$ and $\xi = (3/5)\zeta$). In this regime we assume that the radial scale of the cluster is set by the tidal radius, and so the ratio of the half-mass to tidal radii takes a constant value, which we denote by $(r_{\rm h}/r_{\rm J})_1$. In his equal-mass homological model Hénon (1961) found the value $(r_{\rm h}/r_{\rm J})_1 \simeq 0.145$.

In Fig. 2 we show the behaviour of ξ and χ in units of ζ as a function of $\tau_{\rm cr}/\tau_{\rm cr1}$. The top axis shows how $r_{\rm h}/r_{\rm J}$ relates to $\tau_{\rm cr}/\tau_{\rm cr1}$, which will be explained in more detail in the next subsection (equation 15).

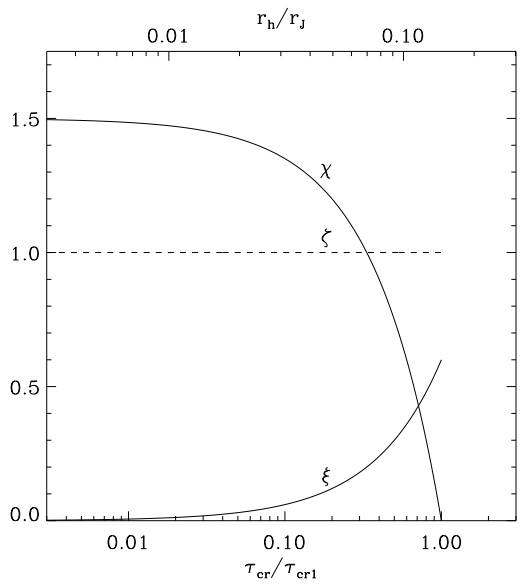

Figure 2. The dependence of the dimensionless escape rate ξ and expansion rate χ on $\tau_{\rm cr}/\tau_{\rm cr1}$ (equations 11 and 12, respectively). The values of χ and ξ are given relative to the efficiency of energy conduction, ζ. The top axis labels corresponding values of $r_{\rm h}/r_{\rm J}$ using equation (15) and $(r_{\rm h}/r_{\rm J})_1 = 0.145$.

2.3 Time scales

Before proceeding to solve the equations of our model for cluster evolution, it is convenient to collect one or two straightforward formulae for future reference. First, we often approximate the half-mass relaxation time (equation 3) by

$$\tau_{\rm rh} \simeq CN\tau_{\rm cr}, \quad (13)$$

where

$$C = \left(\frac{3}{8\pi}\right)^{1/2}\frac{0.138}{\ln\Lambda}, \simeq 0.006. \quad (14)$$

The approximation in the last step is approximately correct if we take $\Lambda = 0.02N$ (Giersz & Heggie 1996) with $N = 10^5$. We turn next to the crossing time $\tau_{\rm cr}$, which is defined in terms of the mean density inside the half-mass radius in Table 1. Since $\tau_{\rm cr} \propto (r_{\rm h}^3/M)^{1/2}$ and $M \propto r_{\rm J}^3$, it follows that $\tau_{\rm cr}$ is related to $r_{\rm h}/r_{\rm J}$ and its value in the evaporation-dominated regime as

$$\frac{\tau_{\rm cr}}{\tau_{\rm cr1}} = \left(\frac{r_{\rm h}/r_{\rm J}}{[r_{\rm h}/r_{\rm J}]_1}\right)^{3/2}. \quad (15)$$

At this point it is also convenient to give an explicit formula for $\tau_{\rm cr1}$, which is

$$\tau_{\rm cr1} = \sqrt{\frac{8\pi r_{\rm J}^3}{3GM}}\left(\frac{r_{\rm h}}{r_{\rm J}}\right)_1^{3/2}. \quad (16)$$

Table 1 also introduces the 'crossing time at the Jacobi radius', which may be expressed as

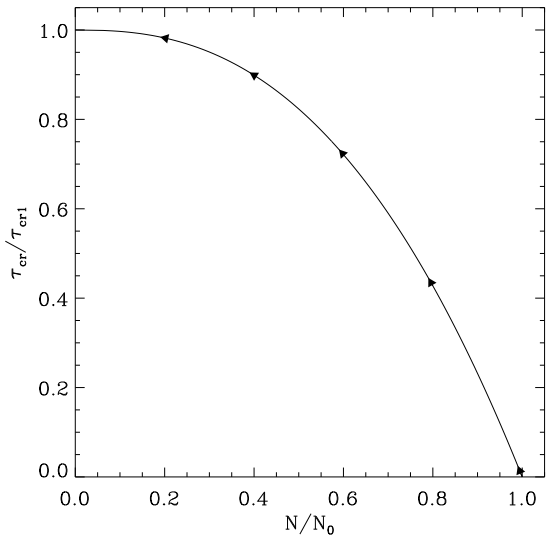

Figure 3. Approximate relation between $\tau_{\rm cr}$ and N, both normalised to their maximum values (equation 19). Evolution is from right to left.

$$\tau_{\rm cr}^{\rm J} = \sqrt{\frac{4\pi r_{\rm J}^3}{3GM}}. \tag{17}$$

Because we now have constrained the functional forms of χ and ξ and we have defined the time-scales involved we can solve for the evolution of $\tau_{\rm cr}(N)$ and the time-dependence of both N and $\tau_{\rm cr}$, and we proceed to do this in the next subsection.

2.4 Motion in the $\tau_{\rm cr} - N$ plane

The evolution of N and $\tau_{\rm cr}$ with respect to one another can be found by combining the descriptions of $\dot{N}$ (equation 11) and $\dot{\tau}_{\rm cr}$ (equation 12) as derived in Section 2.2. This gives us the amazingly simple differential equation

$$\frac{{\rm d}N}{{\rm d}\tau_{\rm cr}} = \frac{2}{5}\frac{N}{\tau_{\rm cr} - \tau_{\rm cr1}}. \tag{18}$$

After separating the variables and integrating we find

$$\tau_{\rm cr} = \tau_{\rm cr1}\left(1 - \left[\frac{N}{N_0}\right]^{5/2}\right), \tag{19}$$

where N_0 is a constant. Strictly, it is the value of N corresponding to $\tau_{\rm cr} = 0$. Our model, however, is intended to describe the phase of balanced evolution, which begins when the cluster is compact, and $\tau_{\rm cr}$ is small but non-zero. But it is easy to see from equation (19) that, when $\tau_{\rm cr}$ is small, $N_0 - N \simeq (2/5)(\tau_{\rm cr}/\tau_{\rm cr1})N_0$. Therefore the value of N at the start of balanced evolution differs little from N_0 provided that the value of $\tau_{\rm cr}$ then is much smaller than $\tau_{\rm cr1}$. Fig. 3 displays the relation between $\tau_{\rm cr}$ and N. The arrows indicate the direction of the motion along the track. The arrows are placed at constant intervals of time and this time dependence will be discussed in Section 2.5.

2.5 Time dependence

Here we complete the solution of equations (8) and (9). The most compact expression of our results will involve the total evolution in time, from the moment when $\tau_{\rm cr} = 0$ until the dissolution of the cluster when $N = 0$. Realistic applications of our model, however, require further consideration of this time scale, and so we take the further development of the model in two stages.

2.5.1 In units of the evaporation time

The time dependence of N and $\tau_{\rm cr}$ can be solved by substituting the expression for $\tau_{\rm rh}$ (equation 13) in the expression for $\dot{N}$ (equation 11), such that we find

$$\dot{N} = -\frac{(3/5)\zeta}{C\tau_{\rm cr1}}, \tag{20}$$

which is constant for a given galactic environment. Thus we get the simple and familiar expression for the time evolution of N

$$N(t) = N_0 + \dot{N}t, \tag{21}$$

$$= N_0\left(1 - \frac{t}{\tau_{\rm ev0}}\right), \tag{22}$$

where $\tau_{\rm ev0}$ is the total life time, which is the time it takes to reduce the number of stars from N_0 to zero. This can be expressed as

$$\tau_{\rm ev0} \equiv -N_0/\dot{N},$$

$$= \frac{\hat{\tau}_{\rm rh}}{(3/5)\zeta}, \tag{23}$$

where $\hat{\tau}_{\rm rh}$ is the relaxation time of a tidally-limited cluster with N_0 stars; i.e. we substitute $N = N_0$ and $\tau_{\rm cr} = \tau_{\rm cr1}$, giving

$$\hat{\tau}_{\rm rh} = CN_0\tau_{\rm cr1}. \tag{24}$$

The time evolution of $\tau_{\rm cr}$ is now retrieved from the expression for $N(t)$ given above and the expression for $\tau_{\rm cr}(N)$ (equation 19), i.e.

$$\tau_{\rm cr}(t) = \tau_{\rm cr1}\left(1 - \left[1 - \frac{t}{\tau_{\rm ev0}}\right]^{5/2}\right). \tag{25}$$

A more familiar quantity, however, is $r_{\rm h}$, whose evolution in time simply follows from the combination of equations (15), (22) and (25), i.e.

$$r_{\rm h}(t) = \hat{r}_{\rm h}\left(1 - \frac{t}{\tau_{\rm ev0}}\right)^{1/3}\left(1 - \left[1 - \frac{t}{\tau_{\rm ev0}}\right]^{5/2}\right)^{2/3} \tag{26}$$

with $\hat{r}_{\rm h} \equiv r_{\rm J0}(r_{\rm h}/r_{\rm J})_1$. Here $r_{\rm J0}$ is the Jacobi radius of a cluster with N_0 stars, and $\hat{r}_{\rm h}$ can be thought of as the half-mass radius the cluster would have had if it still contained N_0 stars and had $\tau_{\rm cr} = \tau_{\rm cr1}$.

Finally, the time evolution of $\tau_{\rm rh}$ (equation 13) is

$$\tau_{\rm rh}(t) = \hat{\tau}_{\rm rh}\left(1 - \frac{t}{\tau_{\rm ev0}}\right)\left(1 - \left[1 - \frac{t}{\tau_{\rm ev0}}\right]^{5/2}\right), \tag{27}$$

with $\hat{\tau}_{\rm rh}$ given in equation (24).

The behaviour of $\tau_{\rm cr}(t), N(t), r_{\rm h}(t)$ and $\tau_{\rm rh}(t)$ is shown in Fig. 4. The point where expansion and evaporation are equally important, i.e. $\xi = \chi$, happens when $t \simeq 0.4\,\tau_{\rm ev0}$. (This is also the time at which the maximum value of $\tau_{\rm rh}$ is reached, as $\tau_{\rm rh} \propto N\tau_{\rm cr}$, if we neglect the variation of the Coulomb logarithm.) Therefore clusters are in an expansion dominated phase for the first 40% of their life, and in an evaporation dominated phase in the following 60%. In Section 3 we will estimate the fraction of globular clusters in the Milky Way that is in the expansion dominated phase. Similarly, we can find the turning point in the evolution of $r_{\rm h}$ from solving $\dot{r}_{\rm h} = 0$ which gives us $t(\dot{r}_{\rm h} = 0) \simeq 0.5\tau_{\rm ev0}$. Therefore $r_{\rm h}$

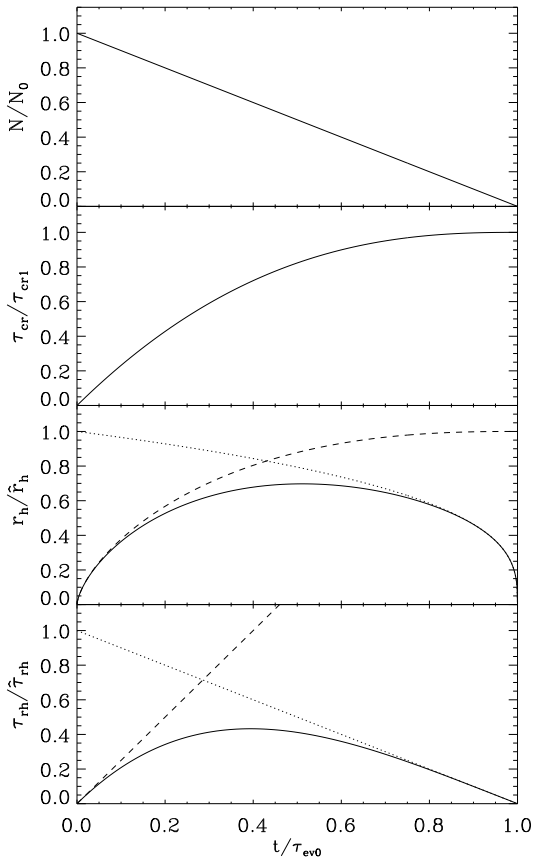

Figure 4. Evolution of the parameters N, $\tau_{\rm cr}$, $r_{\rm h}$ and $\tau_{\rm rh}$ of clusters in a tidal field. Time is normalised to the total evaporation time $\tau_{\rm ev0}$ and the normalisation constants on the y-scale are discussed in the text. The dashed lines in the bottom two panels show the extrapolation of the early evolution assuming that N remains constant. The dotted lines show how $r_{\rm h}$ and $\tau_{\rm rh}$ would have evolved if the evolution would have been homologous throughout: $r_{\rm h}/r_{\rm J} = (r_{\rm h}/r_{\rm J})_1 =$ constant.

increases in the first half of the cluster's life and decreases in the second half.

In the expansion phase, i.e. for $t \ll \tau_{\rm ev0}$, it follows from equation (27) that

$$\tau_{\rm rh}(t) \simeq \frac{5}{2}\left(\frac{\hat{\tau}_{\rm rh}}{\tau_{\rm ev0}}\right) t \simeq \frac{3}{2}\zeta t, \qquad (28)$$

where we have used equations (23) and (24). Hence we arrive at the interesting conclusion that the relaxation time of all such clusters is the same at a given time. Furthermore, since this relationship is represented by the dashed line in the lowest panel of Fig. 4, it is clear that this gives an upper limit on the relaxation time at time t for all clusters satisfying the assumptions of our model. We return to this point in Section 3.3.

2.5.2 In units of physical time

To describe the evolution in units of physical time we need to know the value of $\tau_{\rm ev0}$, which by equations (16) and (23) depends essentially on ζ, $(r_{\rm h}/r_{\rm J})_1$ and the ratio $r_{\rm J}^3/M$ (in addition to N_0). The last of these three quantities is set by the tidal field of the Galaxy, while the first two parameters will be taken as constants, which we shall estimate by comparison with numerical experiments of various kinds.

In isolated models we neglect escape, and then it is easy to show from equations of Section 2.1 that $(\dot{r}_{\rm h}/r_{\rm h})\tau_{\rm rh} \simeq (2/3)\chi \simeq \zeta$. Kim et al. (1998) estimated the value of this quantity for isolated two-component clusters with stars of masses m_1 and m_2, and found, in our notation, that ζ is higher for larger ratios m_2/m_1. More quantitatively, Gieles et al. (2010) use direct N-body integrations to study the expansion of isolated clusters with various mass functions and they find that the dimensionless rate of expansion is approximately proportional to $\mu^{1/2}$, where $\mu \equiv m_{\rm max}/m_{\rm min}$. For $\mu = 10$, appropriate for globular clusters, they find $\chi \simeq 0.3$, i.e. $\zeta \simeq 0.2$.

The result that the efficiency of heat conduction (i.e. ζ) is larger in multi-mass systems is confirmed by studies on the escape rate of tidally-limited clusters. Here we neglect χ, and the equations of Section 2.1 imply that the dimensionless escape-rate is $(\dot{N}/N)\tau_{\rm rh} \simeq -\xi \simeq -(3/5)\zeta$. Lee & Goodman (1995) consider various mass functions in their Fokker-Planck simulations of dissolving clusters and study the effect on the dimensionless escape rate. Strictly, however, their results relate to the rate of escape of mass, i.e. to $(\dot{M}/M)\tau_{\rm rh}$, but we neglect the distinction here. Then for $\mu = 7$ they find that ξ, and thus also ζ, is a factor of $\sim$2 higher than for the equal-mass case. If we assume that $\xi \propto \mu^{1/2}$, then for $\mu = 10$, we again find $\zeta \simeq 0.2$, a value which we adopt henceforth. It is higher than for Hénon's equal-mass models by a factor of ~ 2.5.

Rather than estimating $(r_{\rm h}/r_{\rm J})_1$ directly, we consider the ratio $\zeta/(r_{\rm h}/r_{\rm J})_1^{3/2}$. This can be done by computing the quantity $\dot{N}\tau_{\rm cr}^{\rm J}$ for it follows from equations (16) and (20) that

$$\dot{N}\tau_{\rm cr}^{\rm J} = -\frac{(3/5)\zeta}{\sqrt{2}C(r_{\rm h}/r_{\rm J})_1^{3/2}}. \qquad (29)$$

$$\simeq -\frac{71\,\zeta}{(r_{\rm h}/r_{\rm J})_1^{3/2}}, \qquad (30)$$

where we used $C = 0.006$ in the last step (equation 14). This is the escape rate corrected for the tidal density, and should thus be the same for clusters at different locations in a galaxy. In Table 2 we summarise a number of results on this quantity from the literature, expressed in this way.

For Hénon's equal-mass model ($\zeta \simeq 0.0743$ and $(r_{\rm h}/r_{\rm J})_1 = 0.145$, Sections 2.1 and 2.2) we find $\dot{N}\tau_{\rm cr}^{\rm J} \simeq -95$. The Fokker-Planck models of equal-mass clusters of Lee & Ostriker (1987) start relatively compact, and so nearly the entire evolution of their clusters is spent in the post-collapse phase. Their results imply that $\dot{N}\tau_{\rm cr}^{\rm J} \simeq -76$. On the other hand their values for ξ or ζ (i.e. the escape rate scaled by the half-mass relaxation time, as in equation (8) are slightly larger than Hénon's value. But from their Fig. 2 we see that in their models $(r_{\rm h}/r_{\rm J})_1 \simeq 0.2$, which is slightly larger than the value $(r_{\rm h}/r_{\rm J})_1 = 0.145$ in the model of Hénon. This explains their slightly lower value $\dot{N}\tau_{\rm cr}^{\rm J}$ (equation 30). It also illustrates that ξ is not the only parameter that determines the total life time in physical units.

Note that the results from studies based on N-body simulations in Table 2 have an additional factor proportional to $N^{1/4}$. This N-dependence of the escape rate is reasonably well understood, in terms of the time taken for stars to escape (Baumgardt 2001), and is included in the more refined models in Appendices A and C.

Table 2. Overview of literature results for the escape rate $\dot{N}\tau_{\rm cr}^{\rm J}$ in post-collapse/balanced evolution for clusters with different $\mu \equiv m_{\rm max}/m_{\rm min}$. Values are derived from the results of (1) Hénon (1961) , (2) Lee & Ostriker (1987), (3) Lee, Fahlman & Richer (1991), (4) Heggie et al. (1998), (5) Gieles & Baumgardt (2008), (6) Lamers, Baumgardt & Gieles (2010).

Reference	$-\dot{N}\tau_{\rm cr}^{\rm J}$	μ	Comments
(1)	95	1	Theory
(2)	76	1	Fokker-Planck
(3)	200–250	7	Fokker-Planck
(4)	$290\,\left(N/10^5\right)^{1/4}$	15	N-body
(5)	$300\,\left(N/10^5\right)^{1/4}$	30	N-body
(6)	$270\,\left(N/10^5\right)^{1/4}$	$\sim$10	N-body+stellar evolution

Notes on the data.

(2) Based on their value of A (p.128).

(3) Based on their value of $\tau_{\rm ev}$ (p.458) and a mass-function index $x = 1$.

(4) Based on a run with $N = 65\,536$. The dependence on N has been assumed from Baumgardt (2001).

(5) Based on the results of their Fig. 2. This study found a slightly stronger N-dependence; the $N^{1/4}$ was assumed and matched to the runs with the largest number of particles ($N = 32\,768$).

(6) From a fit to the data presented in their Fig. 4 (Lamers 2010, private communication). This study also finds a slightly stronger N-dependence; the $N^{1/4}$ was again assumed and matched to the runs with the largest number of particles ($N = 131\,072$).

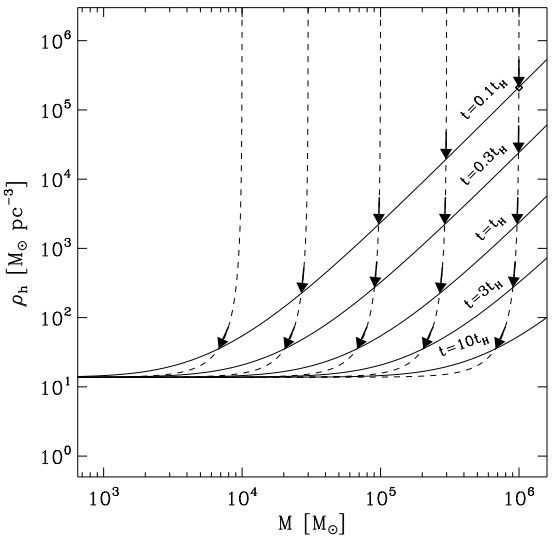

Figure 5. Isochrones (full lines) and evolutionary tracks (dashed lines) extracted from the model described in Section 2, applied to clusters orbiting at a radius of $R_{\rm G} = 8\,{\rm kpc}$ in an isothermal halo with circular velocity of $V_{\rm c} = 220\,{\rm km\,s^{-1}}$. Arrows along the tracks indicate the direction of evolution and have a length of 0.2 dex in time. The central isochrones has an age of a Hubble time $t_{\rm H} = 13\,{\rm Gyr}$.

3 COMPARISON TO THE GLOBULAR CLUSTERS IN THE MILKY WAY

3.1 Model parameters

In this section we compare the basic model of the previous section to parameters of Milky Way globular clusters. We convert the model results for N to M assuming $\bar{m} = 0.5$ and convert $\tau_{\rm cr}$ to $\rho_{\rm h}$ (equation 6). The tidal field parameters $\tau_{\rm cr1}$ and $\tau_{\rm cr}^{\rm J}$ (equations 16 and 17) are converted to $R_{\rm G}$ by approximating the Milky Way potential by that of an isothermal sphere with a (constant) circular velocity of $V_{\rm c} = 220\,{\rm km\,s^{-1}}$ and using Hénon's value $(r_{\rm h}/r_{\rm J})_1 = 0.145$. The resulting formulae are given in Appendix B. With these parameters fixed, the speed of evolution is set by the value of ζ which is chosen to be $\zeta = 0.2$; this is appropriate for clusters with a globular cluster-type mass spectrum ($\mu \simeq 10$, Section 2.5.2). As a consistency check, by equation (30), we derive $\dot{N}\tau_{\rm cr}^{\rm J} \simeq -256$, which may be expressed as (see Appendix B)

$$\dot{M} R_{\rm G} \simeq -20\,{\rm M_\odot\,Myr^{-1}\,kpc}. \quad (31)$$

The first of these is in reasonable agreement with the evaporation rates found in both N-body and Fokker-Planck models with a comparable mass function (Table 2).

From these data we can obtain the value of $\tau_{\rm ev0}$ from substitution into the equations of Section 2.5.1. This then gives us the relation between $\rho_{\rm h}$, M and $R_{\rm G}$ at a given time (isochrones) and the evolution of the individual parameters in time $\rho_{\rm h}(M_0, R_{\rm G}, t)$, $M(M_0, R_{\rm G}, t)$ (tracks). In Appendix B we provide these relations and also some of the intermediate steps and additional relations for $r_{\rm h}(M, R_{\rm G})$ and $r_{\rm h}(M_0, R_{\rm G}, t)$ that are not shown here.

In Fig. 5 we illustrate the behaviour of the evolutionary tracks (dashed lines) together with various isochrones (full lines) in these more appealing quantities for clusters at $R_{\rm G} = 8\,{\rm kpc}$. The isochrones span 2 dex in age centred around a Hubble time ($t_{\rm H} = 13\,{\rm Gyr}$). The asymptotic behaviour of the isochrones at the extremes is easy to understand. In the expansion dominated phase (right-hand side of Fig. 5) all clusters have evolved to the same relaxation time (cf. equation 28) and thus $\rho_{\rm h} \propto (M/t)^2$. The proportionality, i.e. the absolute vertical positioning of the lines, is set by the value of ζ. In the evaporation-dominated regime (left-hand side of Fig. 5) $\rho_{\rm h}$ has adjusted to the tidal density and $\rho_{\rm h} \propto R_{\rm G}^{-2}$. This is because clusters are in the homologous phase where $r_{\rm h}/r_{\rm J} = (r_{\rm h}/r_{\rm J})_1$ and therefore $\rho_{\rm h} \propto \rho_{\rm J}$; while for an isothermal halo the Jacobi density, $\rho_{\rm J}$ scales with $R_{\rm G}$ as $\rho_{\rm J} \propto R_{\rm G}^{-2}$ (Appendix B). The tracks (dashed lines) show that clusters initially move down in this diagram, because they are expanding without losing much mass. Evaporation becomes more important than expansion when $\rho_{\rm h}$ approaches its minimum value and the clusters start moving to the left. In the limit of $t \to \infty$ both the tracks and the isochrones are horizontal lines. The speed of the horizontal motion is set by the value of ζ and $R_{\rm G}$ because it follows from equation (20) that $\dot{M} \propto \zeta/R_{\rm G}$.

3.2 The evolutionary state of Milky Way globular clusters: The relative importance of expansion and evaporation

In order to see if these types of predictions are relevant for real globular clusters we will compare our results to the globular clusters of the Milky Way. We use the 2003 version of the Harris (1996) catalogue. It contains entries for 150 globular clusters, and for 141 of them a luminosity, radius and galacto-centric radius determination are available. To convert luminosity to mass we adopt a mass-to-light ratio of 2 (McLaughlin & van der Marel 2005) and we multiply the projected half-light radius by 4/3 to correct for the effect of projection (Spitzer 1987) and get an estimate for $r_{\rm h}$. Note that by doing this we assume that light traces mass, which is not necessarily true if the cluster is mass segregated (e.g. Lee et al. 1991; Hurley 2007). Bonatto & Bica (2008) study this effect in a sample of 11 globular clusters. They compare the half-light radius to

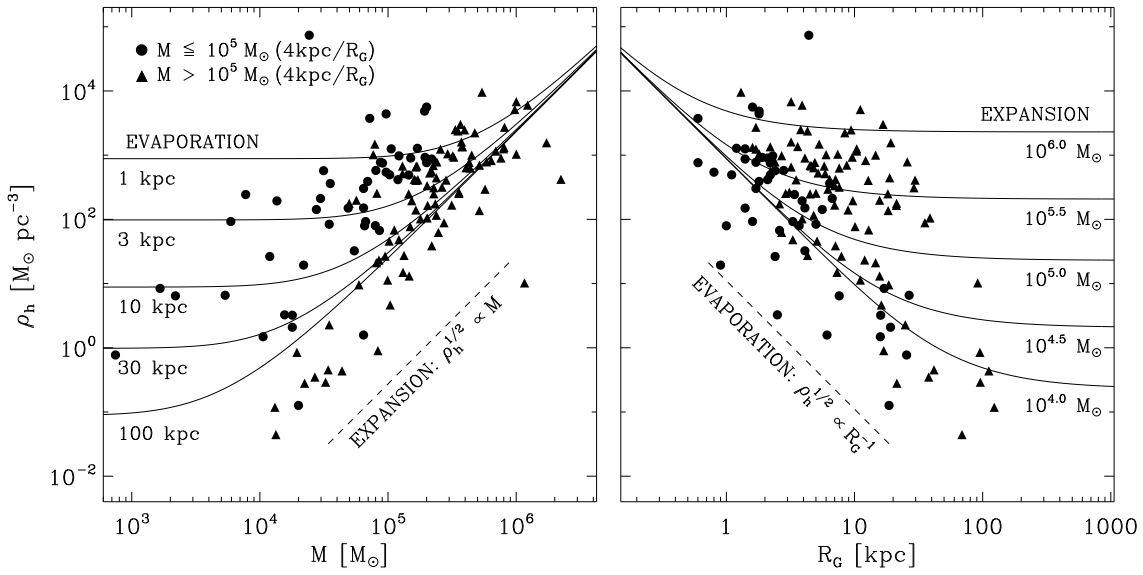

Figure 6. Isochrones based on the balanced evolution models of Section 2. In the left panel 5 isochrones for different $R_{\rm G}$ values are shown and in the right panel 5 isochrones for different M. Both panels show the 141 globular clusters in the Harris (1996) catalogue from which M, $r_{\rm h}$ and $R_{\rm G}$ estimates can be derived. The filled circles are the 48 clusters classified as being in the evaporation-dominated regime according to equation (32). The traingles are the remaining 93 classified as being in the expansion dominated regime.

the radius containing half the number of stars and find that the latter is typically $\sim 10\%$ larger. Hurley (2007) finds from N-body simulations that $r_{\rm h}$ can be about a factor two larger than the projected half-light radius, due to mass segregation. This implies that for some globular clusters $r_{\rm h}$ could be a factor $2/(4/3) = 1.5$ higher than what we derived in Section 3.2. This might affect clusters of different masses in different ways; this is further discussed in Section 4.5. For now we assume that light traces mass and that the correction for projection provides a sufficiently accurate estimate of the 3-dimensional half-mass radius $r_{\rm h}$.

The first thing we determine from the data is the fraction of globular clusters that are in the expansion dominated phase. We adopt the definition of the boundary between these two phases as the moment where the time derivative of $\tau_{\rm rh}$ is zero as outlined in Section 2.5.1. In terms of $\tau_{\rm ev0}$ this point is when the cluster's age is $0.4\tau_{\rm ev0}$ approximately. This means that we need to find the parameters of clusters that at present have a life-expectancy of $\tau_{\rm ev} \simeq 1.5t_{\rm H}$, i.e.with 60% of their evolution still ahead in time. Note that our estimates are based on an assumption that all clusters have spent the last $t_{\rm H}$ at the $R_{\rm G}$ where they are now and that the potential of the Milky Way halo has been constant. This is not generally expected to be true and the consequences of this assumption are discussed in Sections 4.2 and 4.3. The exercise is, therefore, merely intended as a first order approximation to see if it is at all reasonable to expect that globular clusters are still in the expansion phase.

With the adopted model parameters (Section 3.1) and $t_{\rm H} = 13\,{\rm Gyr}$ we find that clusters with

$$M \gtrsim 10^5\,{\rm M}_\odot \left(\frac{4\,{\rm kpc}}{R_{\rm G}}\right) \qquad (32)$$

should still be in the expansion-dominated phase. (Equation 31 is the easiest route to this result.) This relation is satisfied by 93 of the 141 clusters. It follows that the remaining 48 clusters are in the evaporation-dominated phase. This perhaps surprising result has some interesting consequences. The most important one is that the present day densities of the majority of the globular clusters follow (roughly) from the self-similar expansion model for isolated clusters: $\rho_{\rm h} \propto M^2$. Here we have assumed that all clusters have the same age. This scaling relation should be universal, because it is driven by internal 2-body relaxation; therefore a similar scaling, with the same proportionality, should also hold for extra-galactic clusters. Moreover, in extra-galactic cluster samples the fraction of clusters in the expansion-dominated phase is probably larger; they are easier to detect because they have (on average) higher mass (equation 32).

The prediction that a $\rho_{\rm h}^{1/2} \propto M$ scaling must hold for the majority of the Milky Way globular clusters is one of the main results of this paper. More detailed discussion on its implications and consequences are postponed to Section 4. First we show in Section 3.3 that this scaling is indeed found for globular clusters and that the proportionality agrees with the parameters of energy conduction derived in Section 2.

3.3 Isochrones and Milky Way globular clusters

Because all globular clusters have roughly the same age we focus on isochrones with an age of $t_{\rm H} \simeq 13\,{\rm Gyr}$, rather than the evolutionary tracks. In Fig. 6 we show the isochrones in $\rho_{\rm h}\ vs. M$ (left) and $\rho_{\rm h}\ vs. R_{\rm G}$ (right) diagrams together with the 141 globular clusters for which data are available in the Harris catalogue. The clusters that are in the evaporation-dominated phase are shown as filled circles and the clusters that are still expanding are shown as triangles.

In the left panel isochrones for clusters at different $R_{\rm G}$ between 1 kpc and 100 kpc are shown. The isochrones roughly encompass the data. The 100 kpc isochrone clearly shows the asymptotic $\rho_{\rm h}^{1/2} \propto M$ behaviour following from expansion, which

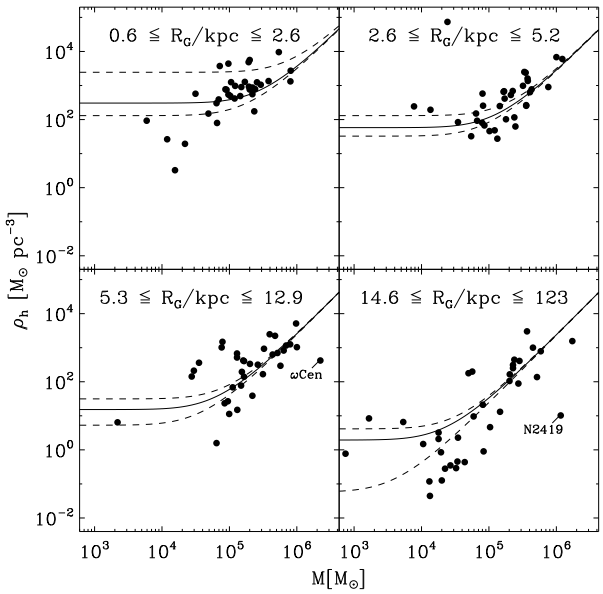

Figure 7. Similar to left panel of Fig. 5, but now the data is sorted in $R_{\rm G}$ and sub-divided in four (roughly) equal samples. The range in $R_{\rm G}$ values is indicated in each panel. The full lines show isochrone predictions for the median $R_{\rm G}$ values in the samples and the dashed lines show the isochrones for the minimum and maximum $R_{\rm G}$ values.

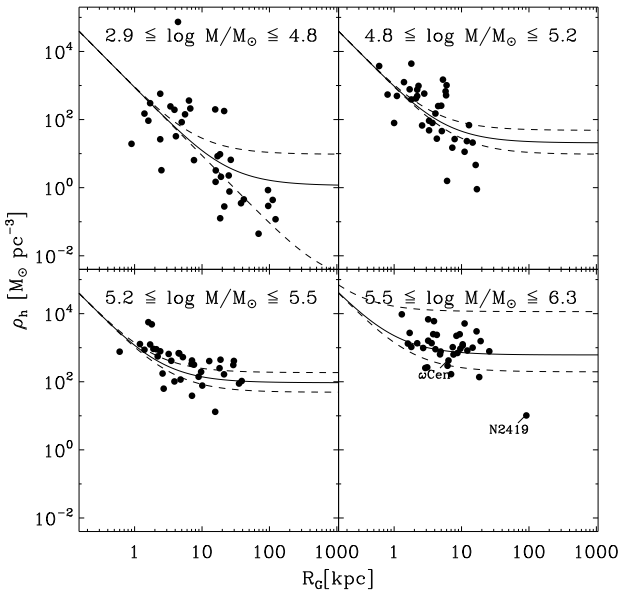

Figure 8. Similar to right panel of Fig. 5, but now the data is sorted in M and sub-divided in four (roughly) equal samples. The range in M values is indicated in each panel. The full lines show isochrones predictions for the median values of M in the samples and the dashed lines show the isochrones for the minimum and maximum values.

roughly follows the lower envelope of data points. In the outer halo the tidal field is so weak that all clusters with $M \gtrsim 10^4\,{\rm M}_\odot$ have not expanded up to their tidal boundary yet. In the right panel the densities are shown as a function of $R_{\rm G}$ together with five isochrones for different masses. As was the case for the isochrones in the $\rho_{\rm h}\,vs.\,M$ plot, these isochrones also roughly encompass the data. The asymptotic behaviour of the isochrones in both diagrams is given by labels in the two diagrams.

To further illustrate the comparison between data and theory we subdivided the Milky Way sample in four samples containing roughly equal numbers, but sorted in M and $R_{\rm G}$. We then compute the isochrones based on the median, the minimum and maximum value in each sample. The results for different $R_{\rm G}$ bins and different M bins are shown in Fig. 7 and Fig. 8, respectively. The general relation between M, $\rho_{\rm h}$ and $R_{\rm G}$ is nicely matched by the model.

Our model is based on the assumption of *balanced* evolution (Section 1), which led to the conclusion that $\tau_{\rm rh} \lesssim 0.3t_{\rm H}$ (Section 2.5.1, equation 28). A logical conclusion of our results, then, is that the evolution of objects with $\tau_{\rm rh} \gtrsim 0.3t_{\rm H}$ is unbalanced, presumably implying that they have formed with a long $\tau_{\rm rh}$ (this scenario was explored using numerical simulations by Hurley & Mackey 2010; Zonoozi et al. 2011). If we draw a hard line at this limit then we find 23 globular clusters for which this holds. However, many of these clusters are fairly close to the $\tau_{\rm rh} = 0.3t_{\rm H}$ line (see left panel of Fig. 6). The majority of the points which are substantially below the lowest isochrone have a low mass, and given the uncertainties in radius, mass and distance estimates for these objects we should not exclude the possibility that their positioning in the diagram is consistent with the model within measurement uncertainties. If these objects are in balanced evolution, they have undergone a lot of dynamical evolution, and could therefore be mass segregated, and perhaps estimates for N, $\bar{m}$ and $r_{\rm h}$ are systematically affected by this. In Section 4 we further discuss this issue of the clusters with $\tau_{\rm rh} \gtrsim 0.3t_{\rm H}$. Obvious exceptions (i.e. high-mass clusters well below the lowest isochrone) are NGC 5139 (ωCen) and NGC 2419 with $\tau_{\rm rh} \simeq 16\,{\rm Gyr}$ and $\tau_{\rm rh} \simeq 54\,{\rm Gyr}$, respectively. These are the only two objects in the Harris catalogues with $\tau_{\rm rh} \gtrsim t_{\rm H}$. Due to their high mass it is unlikely that the data of these objects suffer from measurement uncertainties and it is more likely that these objects have properties resembling their initial conditions (besides some adiabatic expansion because of mass-loss due to stellar evolution perhaps, Hills 1980; Gieles et al. 2010).

4 SUMMARY AND DISCUSSION

In this study we provide a description of the evolution of mass and half-mass density (or radius) of (globular) clusters. The two self-similar solutions provided by Hénon (1965) and Hénon (1961) for clusters evolving in isolation and in a tidal field, respectively, are combined into a pair of Unified Equations of Evolution (UEE), which yield analytically continuous evolutionary tracks and isochrones. The key ingredient is that clusters are assumed to conduct a constant fraction of their total energy per half-mass relaxation time-scale. This is assumption is justified by the fact that both Hénon models, i.e. those that describe the extremes (Hénon 1961, 1965), have a very similar $(\dot{E}/|E|)\tau_{\rm rh} \simeq 0.08$ (see Section 2.1). The central energy source could be assumed to be hard binaries in the centre of the cluster, but the details of the energy production are not of interest to us, since we assume that the evolution is *balanced*, i.e. that the amount of energy produced by the core is determined by how much energy can be conducted through the half-mass boundary. This important view on the evolution of collisional gravitational systems was introduced by Hénon (1975) and can be compared to Eddington's view on stellar energy sources. The bottleneck in the energy emission from a star is the radiative transfer through

the envelope. The luminosity of the star is thus set by how much radiation can be transported through the envelope and the nuclear fusion rate in the core adjusts to this (see Lynden-Bell & Wood 1968 and Inagaki & Lynden-Bell 1983 for more details on this analogy).

The efficiency of energy transport in a cluster depends on the mass spectrum of the stars. For a mass function typical of a globular cluster it is about a factor of ~ 2.5 higher than for the equal mass clusters considered by Hénon. It is this efficiency that determines the positioning of the isochrones and the speed with which clusters move along the tracks. The solutions are compared to the parameters of Milky Way globular clusters and reasonable agreement is found for almost all well-observed clusters. We interpret this agreement as evidence for the fact that the evolution of almost all globular clusters is balanced, meaning that there is a central energy source that supplies the energy needed by 2-body relaxation. Exceptions are NGC 2419 and ωCen because their relaxation timescales are much longer than a Hubble time. The evolution of these clusters is unbalanced. We find that roughly two-thirds of the Milky Way globular clusters are in the expansion dominated phase, i.e. their evolution is not yet seriously affected by the Galactic tidal field. These clusters align along lines of constant relaxation time implying that $\rho_{\rm h} \propto M^2$. This idea is further supported by the properties of intra-cluster globular clusters in the Virgo Cluster, which have no tidal boundary. These have masses of $M \simeq 10^5\,{\rm M}_\odot$ and radii of a few parsecs (Williams et al. 2007), comparable to Milky Way globular clusters.

4.1 Are all globular clusters in post-collapse evolution?

We have referred to balanced evolution when we talked about clusters with a central energy source. For clusters without primordial binaries and stellar evolution this is generally referred to as post-collapse evolution, the energy being provided by binaries formed in three-body interactions. It is interesting to enquire whether these concepts are also related in more realistic models.

At first sight the proportion of Galactic globular clusters which are classified as post-collapse objects is quite inconsistent with our conclusion that the evolution of almost all globular clusters is balanced. Only $\sim 20\%$ of the globular clusters possess the steep cusp in their surface-brightness profile (Djorgovski & King 1986) that is predicted by models of post-collapse evolution. We should bear in mind, however, that such predictions are based on studies of equal-mass systems. In a system with an evolved stellar population, however, it is possible that the distribution of the remnant population is steeply cusped, and that the central distribution of those stars which dominate the surface-brightness exhibits only a shallow cusp. This has been shown in many studies since at least the work on M15 by Illingworth & King (1977); Goodman (1984) gives a general and simple theoretical explanation.

Several independent arguments support the view that the surface-brightness profile is not a reliable guide to the post- or pre-collapse status of a cluster. Cohn & Hut (1984) argued that globular clusters with central relaxation times less than 10^8 yr have already undergone core-collapse, which is close to half of their sample of 146 Galactic globular clusters. Next, De Marchi et al. (2007), on the basis of a surprising correlation between the concentration of a cluster and the slope of the main sequence mass function, argued that the number of post-collapse globular clusters has been seriously underestimated. Finally, specific examples are being revealed by detailed modelling of individual clusters. A good example is the cluster M4, whose surface-brightness profile is well described by a classical King model, but dynamical modelling suggests that it has already undergone core-collapse (Heggie & Giersz 2008).

While these arguments reduce the gap between the proportion of post-collapse clusters, on the one hand, and the proportion exhibiting balanced evolution on the other, they do not imply that the two concepts are identical. In another modelling exercise Giersz & Heggie (2011) argue that 47 Tuc is far from core collapse, and yet the model exhibits what we would call balanced evolution, the required energy being supplied by mass loss from stellar evolution and, to a lesser extent, heating by primordial binaries. In this model, what is called 'core collapse' results from the long-term exhaustion of these energy sources.

Models of globular clusters show an early rapid collapse of the core radius (e.g. Fig.1) caused by mass segregation. It is also exhibited by the model of 47 Tuc which we have just been discussing. This phenomenon is the closest analogue of the classical core collapse exhibited by single-component models, and perhaps the main lesson of this discussion is that we need a better, agreed definition of what we mean by core collapse.

4.2 Cluster orbits

In our model we have made the implicit assumption that cluster orbits are circular in the Milky Way potential. This is of course not true. Dinescu et al. (1999) determined the orbits of 38 globular clusters and they find a median eccentricity of $\epsilon \simeq 0.65$. The question is to what extent this affects our interpretation.

Clusters that are in the expansion-dominated phase are not affected by the tide, and because we have shown that this is the case for the majority of the globular clusters in the Milky Way, the details of the shape of the orbits should not affect the result that the empirically established scaling of $\rho_{\rm h}^{1/2} \propto M$ is a result of expansion. However, our estimate of the fraction of clusters in the expansion dominated phase was based on the assumption of circular orbits. This fraction could very well be smaller because a cluster that is in the expansion phase based on its density and its current galacto-centric position could be in the mass loss dominated phase at peri-centre ($R_{\rm P}$) when we allow for the possibility that $\epsilon > 0$.

Despite what is commonly assumed, conditions at $R_{\rm P}$ are not relevant, either for the structure of the cluster or for the evaporation rate. On the first point, Küpper et al. (2010) showed that the density profile of the bulk of the stars adjusts to the mean tidal radius along the orbit, rather than the tidal radius at perigalacticon. On the second point, again through use of N-body simulations, it has also been shown that the escape rate of a cluster on an oval galactic orbit is close to that of a cluster on a circular orbit with a radius intermediate between $R_{\rm P}$ and the apogalactic distance (Baumgardt & Makino 2003). Though it has not been shown that the galactocentric radius determining the evaporation coincides with that characterising the structure, the systematic error in fitting the evolution of a cluster to its present radius must be considerably smaller than would be the case if structure and mass loss were set at $R_{\rm P}$. Nevertheless, whatever the magnitude of this effect, it does not help to explain those clusters which, in Fig.6 (left panel), lie below the envelope of the isochrones.

4.3 Static galaxy potential

We have assumed that clusters have been evolving for a Hubble time at the galactocentric position where they are observed now. This is an oversimplification, because in the hierarchical merging

scenario clusters can form in dwarf galaxies that are later accreted in larger haloes (Kravtsov & Gnedin 2005; Prieto & Gnedin 2008; Mackey et al. 2010). Most of the galaxies are in place at a redshift $z \simeq 2-3$, hence the assumption of a static galactic potential only affects the clusters that were brought into haloes in late accretion events. In fact, there is the potential of using the densities of clusters to say something about the accretion history. Imagine a cluster in a dwarf galaxy with a strong tidal field. Suppose that in this host it has already reached the evaporation-dominated phase, i.e. its density has adjusted to the tidal density in the dwarf galaxy (which is the case for the clusters associated with the Sagittarius dwarf galaxy, Peñarrubia et al. 2009). If the dwarf galaxy is accreted in a larger host, such as the Milky Way, the new tidal field that the cluster experiences is in most cases weaker than in the previous host. The cluster will start expanding again, but its density is higher than the prediction based on a Hubble time of evolution at that $R_{\rm G}$. A target to which this might apply is Palomar 1 (see the discussion in Niederste-Ostholt et al. 2010).

4.4 Model validity at younger ages

Throughout this study we have assumed a constant value of $\zeta \simeq 0.2$ for all ages. Gieles et al. (2010) found values for ζ as large as 2 for clusters with a full mass spectrum ($\mu = 1000$), which would be appropriate for very young star clusters ($\lesssim 3$ Myr). We have also assumed that the evolution is balanced at all ages. Therefore we need to bear in mind that the results presented here should not be interpreted in a literal way for clusters with ages much younger than a Hubble time. The results presented here underestimate the speed of balanced evolution for younger clusters. For clusters that have not yet reached the balanced evolution phase our results overestimate the speed of evolution. The expansion for clusters with young ages is considered in more detail by Gieles et al. (2010) and we refer to that paper for an analytic description of the radius as a function of initial $\tau_{\rm rh}$ considering the effect of the changing stellar mass function and the transition from un-balanced to balanced evolution. A time-dependent functional form for ζ could in principle be found from the time-dependent parameter χ_t of Gieles et al. (2010). We refrain from doing this, however, because χ_t depends on the details of the stellar mass function, which is affected by both stellar evolution and by the loss of low-mass stars over the tidal boundary. The latter was not taken into account in the models of (Gieles et al. 2010). We therefore leave these details of the full evolution for a future study.

4.5 The stellar mass function

In Section 3.3 we found that there are a number of low-mass clusters with $0.3t_{\rm H} \lesssim \tau_{\rm rh} \lesssim t_{\rm H}$, i.e. their relaxation times seem inconsistent with the predictions for expansion with $\zeta = 0.2$. Several Palomar clusters are in this group. We now consider a number of factors which might account for such cases.

Because these clusters are faint, they could be close to final dissolution and might have stellar mass functions that are depleted in low mass stars (Baumgardt & Makino 2003). We assumed (Section 2.5.2) that the value of ζ, which controls the rate of evolution, depends only on the range of the mass function, i.e. the ratio μ of the maximum to minimum mass, and this does not depend on the slope of the mass function. Gürkan et al. (2004) showed that for the rate of core collapse it is not $\mu = m_{\rm max}/m_{\rm min}$ that sets the speed of evolution, but rather $m_{\rm max}/\bar{m}$, where $\bar{m}$ is the mean mass. If the same consideration applies to balanced evolution, then for flatter mass spectra, i.e. lower $m_{\rm max}/\bar{m}$, we would expect a slower dynamical evolution, i.e. smaller ζ. By equation (23) this increases the ratio $\tau_{\rm ev0}/\tau_{\rm cr1}$. By use of equation (24) we see from equation (28) that the effect is to reduce the ratio $\tau_{\rm rh}/t$ in the expansion phase. Thus for a given mass, clusters should be denser at a given age. On the other hand Fig.6 (left panel) shows that the clusters of concern are less dense than expected. We conclude, therefore, that a flatter mass function can not be responsible for an additional decrease of the densities of these low mass clusters.

Another consideration is the N-dependence in the escape rate which is implicit in the N-body results quoted in Table 2. This affects the expansion rate χ of clusters that are well into the evaporation-dominated regime (Appendix A) and therefore does not help us to understand the discrepant objects.

We propose two alternative speculative explanations. Firstly, it could be that these clusters had a high retention fraction of black holes and neutron stars. If the most massive stars are black holes with $m \simeq 10-20\,{\rm M}_\odot$, the ratio μ would be higher and the dynamical evolution would be faster. As mentioned in Section 2.5.2, Gieles et al. (2010) show that $\zeta \propto \mu^{1/2}$ approximately. For a mass function between $0.1\,{\rm M}_\odot$ and $1\,{\rm M}_\odot$ we have adopted $\zeta \simeq 0.2$. For a cluster with a few additional black holes with masses of $10\,{\rm M}_\odot$ we would have ζ approximately a factor of ~ 3 higher. This would help to make all of these clusters consistent with balanced evolution.

Secondly, we have assumed that the mass-to-light ratio is the same for all clusters. But if the cluster is depleted in low-mass stars we surely overestimate N and underestimate $\bar{m}$ by using a canonical mass-to-light ratio. Because $\tau_{\rm rh} \propto (N/\bar{m})^{1/2}$ we thus overestimate $\tau_{\rm rh}$. Thus if, according to our estimates, a cluster has a half-mass relaxation time-scale $> 0.3t_{\rm H}$, it may be that its actual $\tau_{\rm rh}$ is more consistent with our theory. It would be interesting to consider these effects in more detail with numerical simulations.

Lastly, estimates of $\tau_{\rm rh}$ are very sensitive to uncertainties in the distance to the cluster, D. The radius in pc depends linearly on D and the mass in solar masses quadratically, such that $\tau_{\rm rh} \propto D^{5/2}$. Because $\rho_{\rm h} \propto D^{-1}$ and $M \propto D^2$ the scatter of data points due to uncertainties in D is orthogonal to lines of constant relaxation time (left panel of Fig. 6 and Fig. 7).

4.6 Comparison to other work

The relation of globular clusters to lines of constant relaxation time ($\rho_{\rm h}^{1/2} \propto M$) has been noted for Milky Way globular clusters and for extra-galactic globular clusters (e.g. Gnedin & Ostriker 1997; Barmby et al. 2007; McLaughlin & Fall 2008; Georgiev et al. 2009). It is usually given a different interpretation, however. Because for homologous clusters the life-expectancy is a constant number of relaxation times ($1/\xi$) the lines of constant $\tau_{\rm rh}$ have been interpreted as *boundaries* to the expected distribution of surviving clusters. The first to provide this interpretation were probably Fall & Rees (1977) who showed the dependence on mass and radius of various disruptive agents. Given that the time-scales for relaxation driven evaporation (of homologous clusters), disruption by tidal shocks and dynamical friction all depend in a different way on cluster mass and radius one can construct a 'survival' or 'vital' triangle in an $r_{\rm h} vs. M$ diagram (e.g. Gnedin & Ostriker 1997), or alternatively $\rho_{\rm h} vs. M$. Clusters within this triangle are likely to survive for another Hubble time.

In this paper we have given a different interpretation to the re-

lation between cluster data and lines of constant $\tau_{\rm rh}$. Because the majority of the clusters have not reached the homologous (tidally limited) evaporation-dominated phase yet, the alignment of the globular cluster data for these clusters with the $\tau_{\rm rh} \simeq 0.3t_{\rm H}$ relation results from expansion driven by 2-body relaxation when evolution is balanced. There would be no globular clusters with shorter relaxation times if there was no tidal field that can stop the expansion. In reality clusters can not expand indefinitely, and the relaxation time starts decreasing once evaporation starts to dominate over expansion. This is why there are clusters with $\tau_{\rm rh} < 0.3t_{\rm H}$. Note that this is just the opposite of the usual interpretation, which implies that only clusters with *longer* relaxation times should be observed!

Because $\tau_{\rm rh}$ decreases linearly in time in the homologous phase, there should be a uniform distribution of $\tau_{\rm rh}$ values between 0 and $\sim 0.3t_{\rm H}$. This was proposed by Lee & Goodman (1995) and they show that this indeed roughly holds. Since in the homologous phase $\tau_{\rm rh} \propto M$, there should also be a uniform distribution of M at low mass, or ${\rm d}N/{\rm d}M \simeq$ const (Hénon 1961; Fall & Zhang 2001), which is indeed found in many galaxies (Jordán et al. 2007).

Küpper et al. (2008) recently presented results of N-body simulations of initial compact clusters in a tidal field. They refer to the phase where the half-mass radius has adjusted to the Jacobi radius as 'main sequence' evolution. Using again the analogy with stars we could, however, refer to the entire balanced evolution, i.e. expansion and evaporation, as main sequence evolution. The initial unbalanced evolution without a central energy source would then be the 'pre-main sequence evolution'. On the other hand perhaps the analogy should not be pushed too far; for Lynden-Bell & Wood (1968) the end of core collapse signalled the start of the red giant phase!

Baumgardt et al. (2010) identified two populations of clusters based on the ratio of the half-mass radius over the Jacobi radius ($r_{\rm h}/r_{\rm J}$). About half of the clusters beyond $\gtrsim 8\,{\rm kpc}$ is strongly under-filling their tidal radius (i.e. $r_{\rm h} << r_{\rm J}$), while the other half have $0.1 \lesssim r_{\rm h}/r_{\rm J} \lesssim 0.3$. They find a strong correlation between mass and the membership of these groups: the under-filling group contains significantly more-massive clusters than the 'tidally filling' group. This separation is because low-mass clusters have already expanded towards their tidal boundary and all have a similar ratio $r_{\rm h}/r_{\rm J}$. Their more massive counterparts are still expanding towards their tidal boundary (see right panel of Fig. 6). The densities of clusters in the expansion-dominated regime within $R_{\rm G} \lesssim 8\,{\rm kpc}$ are more similar to those of the clusters that are already in the evaporation-dominated regime (Fig. 6) and it is, therefore, harder to make a distinction between under-filling and filling based on the empirically determined ratio $r_{\rm h}/r_{\rm J}$.

4.7 Implications for the use of globular clusters as standard rulers for distance estimation

Globular cluster properties have been used as standard candles for distance estimates. Traditionally the peak of the globular cluster luminosity function (GCLF), because of its near universality, is used for this (e.g. Harris 1991). However, even *if* the initial mass function of globular clusters is universal, the detailed shape of the GCLF will be environment dependent after a Hubble time of dynamical evolution (Vesperini & Heggie 1997; Ostriker & Gnedin 1997; Villegas et al. 2010). Jordán et al. (2005) suggested that the radius distribution can be used as a standard ruler. Alternatively, we suggest to use a combination of the two as a distance ruler; namely the relation between apparent luminosity and radius. This can be done because for the majority of clusters the mass-radius relation is independent of environment and second order effects such as the stellar mass function can in principle be taken into account (see also Jordán 2004).

4.8 Relation to fundamental plane relations

With all the theory in place we are able to test if empirically established 'fundamental-plane relations' (e.g. Djorgovski 1995; Burstein et al. 1997; McLaughlin 2000) can be attributed to balanced evolution. Because we do not make predictions for the central velocity dispersion, we will focus here on the mass-radius relation.

It is often stated that the radii of globular clusters do not correlate with their mass (e.g. van den Bergh et al. 1991). This statement is perhaps a slight oversimplification, because there may be a negative correlation, especially for clusters in the outer halo (van den Bergh & Mackey 2004; Baumgardt et al. 2010). McLaughlin (2000) showed that, if a correction is made for the galacto-centric radius, the cluster half-mass radius is approximately constant, i.e. independent of mass: $r_{\rm h}/R_{\rm G}^{0.4} \sim$ constant.

Strictly speaking the theory presented in this paper can not explain a radius that is perfectly independent of mass. The relation between mass and half-mass radius depends on the regime the cluster is in. For clusters in the expansion dominated regime we expect a constant relaxation time, i.e. $r_{\rm h} \propto M^{-1/3}$ independent of $R_{\rm G}$, while for clusters in the mass loss regime we expect a stronger dependence on $R_{\rm G}$ than on M: $r_{\rm h} \propto M^{1/3}R_{\rm G}^{2/3}$ (or $r_{\rm h} \propto M^{1/6}R_{\rm G}^{2/3}$ when we use a slightly different escape criterion, see Appendix A). [3].

If we split the Milky Way globular cluster sample, using the boundary between these two extremes as described in Section 3.2, then we can search for these different (bivariate) relations in the data and see if they indeed hold. We use a straightforward linear regression fit to find how $\log r_{\rm h}$ depends on $\log M$ and $\log R_{\rm G}$. We exclude ωCen and NGC 2419 because the balanced evolution does not apply to these objects. We also exclude NGC 6540, with a density of $\rho_{\rm h} \simeq 7\times10^4\,{\rm M}_\odot{\rm pc}^{-3}$, because it is an extreme outlier in all diagrams. From a bivariate fit to the 47 clusters in the evaporation-dominated regime we find

$$\begin{aligned}\log(r_{\rm h}/{\rm pc}) &= -0.16 + (0.11\pm0.08)\log(M/{\rm M}_\odot) \\ &\quad +(0.44\pm0.11)\log(R_{\rm G}/{\rm kpc}).\end{aligned} \tag{33}$$

This shows a weak positive correlation with M close to the predicted index of $0.17(0.33)$ for $x = 3/4(1)$ (see Appendices A and C for the significance of x) and a relatively strong dependence on $R_{\rm G}$, in rather poorer agreement with the predicted index of 0.67. On the other hand we find for the 91 clusters in the expansion dominated regime

$$\begin{aligned}\log(r_{\rm h}/{\rm pc}) &= 1.82 - (0.25\pm0.05)\log(M/{\rm M}_\odot) \\ &\quad +(0.27\pm0.05)\log(R_{\rm G}/{\rm kpc}).\end{aligned} \tag{34}$$

This is consistent with a constant relaxation time ($r_{\rm h} \propto M^{-1/3}$,

[3] The correlation between $r_{\rm h}$ and M becomes weaker still if we take into account the Coulomb logarithm. If we approximate $\ln\Lambda$ by a weak power of M: $\ln\Lambda \propto M^{0.15}$ then we find in the expansion dominated regime that $r_{\rm h} \propto \ln\Lambda^{2/3}M^{-1/3} \simeq M^{-0.23}$ and in the evaporation dominate regime $r_{\rm h} \propto M^{1/3}/\ln\Lambda^{2/3} \simeq M^{0.23}$ (or $r_{\rm h} \propto M^{1/6}/\ln\Lambda^{2/3} \simeq M^{0.07}$ for $x = 3/4$, see Appendix A).

equation 3), but there is still some dependence on $R_{\rm G}$, whereas pure expansion would not give rise to any $R_{\rm G}$ dependence.

The balanced evolution we consider here is thus responsible for a slightly complicated correlation between radius and mass. The theory predicts that the radius has a slight positive correlation with mass for $M \leqslant 10^5\,{\rm M}_\odot(4\,{\rm kpc}/R_{\rm G})$, while for more massive clusters the correlation is negative and consistent with a constant relaxation time relation. This subtle behaviour of the mass-radius relation is indeed found (at least qualitatively) for the Milky Way globular clusters, as we have just seen. An approximately mass-independent radius (at a given $R_{\rm G}$) is thus only true to first approximation for the population as a whole. The strong correlation of $r_{\rm h}$ with $R_{\rm G}$ for the cluster population as a whole does not seem consistent with our finding that the majority of the clusters are still expanding. However, we note that the scaling $r_{\rm h} \propto R_{\rm G}^{0.4}$ is very sensitive to the handful of very low density clusters in the outer halo ($\gtrsim 50\,R_{\rm G}$).

ACKNOWLEDGEMENT

MG acknowledges the Royal Society for financial support and the School of Mathematics of the University of Edinburgh for several pleasant visits. The authors thank Florent Renaud for providing translations into English of the two seminal papers of Michel Hénon and for various interesting discussions on the effect of tides on star clusters. The authors also thank the referee, Donald Lynden-Bell, for interesting suggestions and comments on the manuscript.

REFERENCES

Barmby P., McLaughlin D. E., Harris W. E., Harris G. L. H., Forbes D. A., 2007, AJ, 133, 2764
Baumgardt H., 2001, MNRAS, 325, 1323
Baumgardt H., Hut P., Heggie D. C., 2002, MNRAS, 336, 1069
Baumgardt H., Makino J., 2003, MNRAS, 340, 227
Baumgardt H., Makino J., Ebisuzaki T., 2004, ApJ, 613, 1143
Baumgardt H., Parmentier G., Gieles M., Vesperini E., 2010, MNRAS, 401, 1832
Bonatto C., Bica E., 2008, A&A, 479, 741
Burstein D., Bender R., Faber S., Nolthenius R., 1997, AJ, 114, 1365
Cohn H., 1979, ApJ, 234, 1036
Cohn H., Hut P., 1984, ApJ, 277, L45
De Marchi G., Paresce F., Pulone L., 2007, ApJ, 656, L65
Dinescu D. I., Girard T. M., van Altena W. F., 1999, AJ, 117, 1792
Djorgovski S., 1995, ApJ, 438, L29
Djorgovski S., King I. R., 1986, ApJ, 305, L61
Fall S. M., Rees M. J., 1977, MNRAS, 181, 37P
Fall S. M., Zhang Q., 2001, ApJ, 561, 751
Fukushige T., Heggie D. C., 2000, MNRAS, 318, 753
Georgiev I. Y., Puzia T. H., Hilker M., Goudfrooij P., 2009, MNRAS, 392, 879
Gieles M., Baumgardt H., 2008, MNRAS, 389, L28
Gieles M., Baumgardt H., Heggie D. C., Lamers H. J. G. L. M., 2010, MNRAS, 408, L16
Giersz M., Heggie D. C., 1994, MNRAS, 268, 257
Giersz M., Heggie D. C., 1996, MNRAS, 279, 1037
Giersz M., Heggie D. C., 2011, MNRAS, 410, 2698
Gnedin O. Y., Ostriker J. P., 1997, ApJ, 474, 223
Goodman J., 1984, ApJ, 280, 298
Gürkan M. A., Freitag M., Rasio F. A., 2004, ApJ, 604, 632
Harris W. E., 1991, ARA&A, 29, 543
Harris W. E., 1996, AJ, 112, 1487
Harris W. E., Spitler L. R., Forbes D. A., Bailin J., 2010, MNRAS, 401, 1965
Heggie D. C., Giersz M., 2008, MNRAS, 389, 1858
Heggie D. C., Giersz M., Spurzem R., Takahashi K., 1998, Highlights of Astronomy, 11, 591
Hénon M., 1961, Annales d'Astrophysique, 24, 369
Hénon M., 1965, Annales d'Astrophysique, 28, 62
Hénon M., 1975, in A. Hayli, ed., Proc. IAU Symp. 69, Dynamics of the Solar Systems. Reidel, Dordrecht, p. 133
Hills J. G., 1980, ApJ, 235, 986
Hurley J. R., 2007, MNRAS, 379, 93
Hurley J. R., Mackey A. D., 2010, MNRAS, 408, 2353
Illingworth G., King I. R., 1977, ApJ, 218, L109
Inagaki S., Lynden-Bell D., 1983, MNRAS, 205, 913
Jordán A., 2004, ApJ, 613, L117
Jordán A., Côté P., Blakeslee J. P., Ferrarese L., McLaughlin D. E., Mei S., Peng E. W., Tonry J. L., Merritt D., Milosavljević M., Sarazin C. L., Sivakoff G. R., West M. J., 2005, ApJ, 634, 1002
Jordán A., McLaughlin D. E., Côté P., Ferrarese L., Peng E. W., Mei S., Villegas D., Merritt D., Tonry J. L., West M. J., 2007, ApJS, 171, 101
Kim S. S., Lee H. M., Goodman J., 1998, ApJ, 495, 786
Kravtsov A. V., Gnedin O. Y., 2005, ApJ, 623, 650
Küpper A. H. W., Kroupa P., Baumgardt H., 2008, MNRAS, 389, 889
Küpper A. H. W., Kroupa P., Baumgardt H., Heggie D. C., 2010, MNRAS, 407, 2241
Lamers H. J. G. L. M., Baumgardt H., Gieles M., 2010, MNRAS, 409, 305
Lee H. M., 2002, in D. P. Geisler, E. K. Grebel, & D. Minniti ed., Proc. IAU Symp. 207, Extragalactic Star Clusters, Astron. Soc. Pac., San Francisco, p. 584
Lee H. M., Fahlman G. G., Richer H. B., 1991, ApJ, 366, 455
Lee H. M., Goodman J., 1995, ApJ, 443, 109
Lee H. M., Ostriker J. P., 1987, ApJ, 322, 123
Lynden-Bell D., Wood R., 1968, MNRAS, 138, 495
Mackey A. D., Huxor A. P., Ferguson A. M. N., Irwin M. J., Tanvir N. R., McConnachie A. W., Ibata R. A., Chapman S. C., Lewis G. F., 2010, ApJ, 717, L11
McLaughlin D. E., 2000, ApJ, 539, 618
McLaughlin D. E., Barmby P., Harris W. E., Forbes D. A., Harris G. L. H., 2008, MNRAS, 384, 563
McLaughlin D. E., Fall S. M., 2008, ApJ, 679, 1272
McLaughlin D. E., van der Marel R. P., 2005, ApJS, 161, 304
Niederste-Ostholt M., Belokurov V., Evans N. W., Koposov S., Gieles M., Irwin M. J., 2010, MNRAS, 408, L66
Ostriker J. P., Gnedin O. Y., 1997, ApJ, 487, 667
Peñarrubia J., Walker M. G., Gilmore G., 2009, MNRAS, 399, 1275
Portegies Zwart S., Gaburov E., Chen H., Gürkan M. A., 2007, MNRAS, 378, L29
Prieto J. L., Gnedin O. Y., 2008, ApJ, 689, 919
Spitzer L., 1987, Dynamical evolution of globular clusters. Princeton, NJ, Princeton University Press, 1987, 191 p.
Spitzer L. J., 1969, ApJ, 158, L139
van den Bergh S., Mackey A. D., 2004, MNRAS, 354, 713
van den Bergh S., Morbey C., Pazder J., 1991, ApJ, 375, 594
Vesperini E., Heggie D. C., 1997, MNRAS, 289, 898

Villegas D., Jordán A., Peng E. W., Blakeslee J. P., Côté P., Ferrarese L., Kissler-Patig M., Mei S., Infante L., Tonry J. L., West M. J., 2010, ApJ, 717, 603
Williams B. F., Ciardullo R., Durrell P. R., Feldmeier J. J., Sigurdsson S., Vinciguerra M., Jacoby G. H., von Hippel T., Ferguson H. C., Tanvir N. R., Arnaboldi M., Gerhard O., Aguerri J. A. L., Freeman K. C., 2007, ApJ, 654, 835
Zonoozi A. H., Küpper A. H. W., Baumgardt H., Haghi H., Kroupa P., Hilker M., 2011, MNRAS, 411, 1989

APPENDIX A: ALTERNATIVE ESCAPE CRITERION

In Section 2 we have solved the simple case in which the escape rate is constant during the entire evolution. This resulted from the fact that we used the scaling $\xi \propto \tau_{\rm cr}$, cancelling out the $\tau_{\rm cr}$ term of $\tau_{\rm rh}$ in equation (11). The constant escape rate is to first order a good approximation, but a slightly improved description for ξ would be the exponential function mentioned in Section 2.2. In principle all derivations of Section 2 can be repeated using different functional forms for ξ. Together with the constraint that $\zeta =$ constant we can always solve for χ. For the exponential function mentioned before we would have to proceed with numerical integrations of the various differential equations, which we will not do here.

Stars that have enough energy to escape take a finite time to do so, and this has a profound effect on the escape rate. This time scale can be very long for stars with energies only slightly higher than the escape energy (Fukushige & Heggie 2000). We will not discuss the details of the theory here and instead proceed directly to the consequences for the escape rate. This was considered by Baumgardt (2001) and he has shown that the relevant time-scale for escape is in fact a combination of $\tau_{\rm rh}$ and $\tau_{\rm cr}$

$$\tau_{\rm esc} \propto \tau_{\rm rh}^{x}\tau_{\rm cr}^{1-x} \quad (A1)$$

$$\propto \tau_{\rm rh}\left(\frac{\tau_{\rm cr}}{\tau_{\rm rh}}\right)^{1-x}, \quad (A2)$$

i.e.

$$\tau_{\rm esc} \simeq \tau_{\rm rh}\left(\frac{N}{N_1}\right)^{x-1}, \quad (A3)$$

with $x \simeq 3/4$. The proportionality, i.e. the value of the reference number N_1, may be determined by matching the time scales following from the theory to the results of N-body simulations. We again define the dimensionless escape-rate ξ as the fraction of stars lost per relaxation time such that an additional (small) N-dependence needs to be included; thus instead of equation (11) we have

$$\xi \equiv -\frac{\dot{N}\tau_{\rm rh}}{N} = \frac{3}{5}\zeta\left(\frac{\tau_{\rm cr}}{\tau_{\rm cr1}}\right)\left(\frac{N}{N_1}\right)^{1-x}. \quad (A4)$$

The escape rate corrected for the tidal density then becomes

$$\dot{N}\tau_{\rm cr}^{\rm J} = -\frac{71\zeta}{(r_{\rm h}/r_{\rm J})_1^{3/2}}\left(\frac{N}{N_1}\right)^{1-x} \quad (A5)$$

in place of equation (30). Consequently the N-dependence also enters in the expression for χ through the constraint that ζ is constant (equation 10)

$$\chi \equiv \frac{\dot{\tau}_{\rm cr}\tau_{\rm rh}}{\tau_{\rm cr}} = \frac{3}{2}\zeta\left(1-\frac{\tau_{\rm cr}}{\tau_{\rm cr1}}\left[\frac{N}{N_1}\right]^{1-x}\right), \quad (A6)$$

in place of equation (12).

A1 Motion in the $\tau_{\rm cr} - N$ plane

The motion in the $\tau_{\rm cr} - N$ plane can be found in a similar way as in Section 2.4. With $\dot{N}$ and $\dot{\tau}_{\rm cr}$ defined as in equations (A4) and (A6) we then find

$$\frac{{\rm d}N}{{\rm d}\tau_{\rm cr}} = -\frac{\xi}{\chi}\frac{N}{\tau_{\rm cr}} = \frac{2}{5}\frac{N^{2-x}}{\tau_{\rm cr}N^{1-x} - \tau_{\rm cr1}N_1^{1-x}}. \quad (A7)$$

Because the variables $\tau_{\rm cr}$ and N can not be separated, a variable substitution $u = \tau_{\rm cr}N^{1-x}$ needs to be performed and then the variables u and N can be separated and the integration can be performed. The result is

$$\tau_{\rm cr} = \frac{\tau_{\rm cr1}}{A}\left(\frac{N}{N_1}\right)^{x-1}\left(1-\left[\frac{N}{N_0}\right]^{5A/2}\right). \quad (A8)$$

Here $A \equiv 1 + (2/5)(1-x)$ and we again used $\tau_{\rm cr0} = 0$. When $x = 1$, then $A = 1$ and equation (A8) reduces to the result of Section 2 (equation 19).

The continuous growth of $\tau_{\rm cr}$ with decreasing N in the tidal regime shows that clusters are not evolving homologically any more in the evaporation dominated regime. This is different from the model of Hénon where $\tau_{\rm cr}$ becomes a constant related to the tidal density. The time-dependence also changes and this is discussed in A2.

A2 Time-dependence

The time-dependence of the evolution can be found as before from an integration over $\dot{N}$ (equation A5)

$$N(t) = N_0\left(1-\frac{t}{\tau_{\rm ev0}}\right)^{1/x}, \quad (A9)$$

with $\tau_{\rm ev0}$ now defined as

$$\tau_{\rm ev0} = \frac{(r_{\rm h}/r_{\rm J})_1^{3/2}}{71\zeta}\frac{N_1^{1-x}}{x}\tau_{\rm cr}^{\rm J}N_0^{x}. \quad (A10)$$

The time-dependent $\tau_{\rm cr}(t)$ follows from equation (A8) and the above. We can then also get $r_{\rm h}(t)$ and $\tau_{\rm rh}(t)$, but this will not be done here.

APPENDIX B: TRACKS AND ISOCHRONES IN UNITS OF M, $\rho_{\rm h}$ AND $R_{\rm G}$

In this appendix we present the results of Section 2 in terms of M, $\rho_{\rm h}$ and $\rho_{\rm J}$. We return to the case $x = 1$.

B1 Tracks

The evolution of mass is

$$M(M_0, t) = M_0 - |\dot{M}|t \quad (B1)$$

If we use $\bar{m} = 0.5$ then from equations (16) and (20) we find

$$|\dot{M}| \simeq 35.4\zeta\left(\frac{G\rho_{\rm J}}{[r_{\rm h}/r_{\rm J}]_1^3}\right)^{1/2}. \quad (B2)$$

Together with equations (22) and (25) we then have for the density

$$\rho_{\rm h}(\rho_{\rm J},M_0,t) = \frac{1}{2}\left(\frac{r_{\rm h}}{r_{\rm J}}\right)_1^{-3}\rho_{\rm J}\left(1-\left[1-\frac{|\dot{M}|t}{M_0}\right]^{5/2}\right)^{-2}, \quad \text{(B3)}$$

$$\rho_{\rm h}(M_0,t) \simeq \frac{1}{G}\left(\frac{M_0}{125\zeta t}\right)^2, \quad M_0 \gg |\dot{M}|t, \quad \text{(B4)}$$

$$\rho_{\rm h}(\rho_{\rm J},M_0,t) \simeq \frac{1}{2}\left(\frac{r_{\rm h}}{r_{\rm J}}\right)_1^{-3}\rho_{\rm J}, \quad M_0 \simeq |\dot{M}|t, \quad \text{(B5)}$$

or in terms of radius

$$r_{\rm h}(\rho_{\rm J},M_0,t) = \left(\frac{6}{8\pi}\right)^{1/3}\left(\frac{r_{\rm h}}{r_{\rm J}}\right)_1\left(\frac{M_0}{\rho_{\rm J}}\right)^{1/3}\left(1-\frac{|\dot{M}|t}{M_0}\right)^{1/3} \times\left(1-\left[1-\frac{|\dot{M}|t}{M_0}\right]^{5/2}\right)^{2/3}, \quad \text{(B6)}$$

$$r_{\rm h}(M_0,t) \simeq \left(\frac{3G}{8\pi M_0}\right)^{1/3}(125\zeta t)^{2/3}, \quad M_0 \gg |\dot{M}|t, \quad \text{(B7)}$$

$$r_{\rm h}(\rho_{\rm J},M_0,t) \simeq \left(\frac{6}{8\pi}\right)^{1/3}\left(\frac{r_{\rm h}}{r_{\rm J}}\right)_1\left(\frac{M_0}{\rho_{\rm J}}\right)^{1/3} \times\left(1-\frac{\dot{M}t}{M_0}\right)^{1/3}, \quad M_0 \simeq |\dot{M}|t. \quad \text{(B8)}$$

B2 Isochrones

The isochrones are easily found from the tracks and using $M_0 = M + |\dot{M}|t$

$$\rho_{\rm h}(\rho_{\rm J},M,t) = \frac{1}{2}\left(\frac{r_{\rm h}}{r_{\rm J}}\right)_1^{-3}\rho_{\rm J}\left(1-\left[1+\frac{|\dot{M}|t}{M}\right]^{-5/2}\right)^{-2}, \quad \text{(B9)}$$

$$\rho_{\rm h}(M,t) \simeq \frac{1}{G}\left(\frac{M}{125\zeta t}\right)^2, \quad M \gg |\dot{M}|t, \quad \text{(B10)}$$

$$\rho_{\rm h}(\rho_{\rm J},M) \simeq \frac{1}{2}\left(\frac{r_{\rm h}}{r_{\rm J}}\right)_1^{-3}\rho_{\rm J}, \quad M \simeq |\dot{M}|t, \quad \text{(B11)}$$

or in terms of radius

$$r_{\rm h}(\rho_{\rm J},M,t) = \left(\frac{6}{8\pi}\right)^{1/3}\left(\frac{r_{\rm h}}{r_{\rm J}}\right)_1\left(\frac{M}{\rho_{\rm J}}\right)^{1/3} \times\left(1-\left[1+\frac{|\dot{M}|t}{M}\right]^{-5/2}\right)^{2/3}, \quad \text{(B12)}$$

$$r_{\rm h}(M,t) \simeq \left(\frac{3G}{8\pi M}\right)^{1/3}(125\zeta t)^{2/3}, M \gg |\dot{M}|t, \quad \text{(B13)}$$

$$r_{\rm h}(\rho_{\rm J},M) \simeq \left(\frac{6}{8\pi}\right)^{1/3}\left(\frac{r_{\rm h}}{r_{\rm J}}\right)_1\left(\frac{M}{\rho_{\rm J}}\right)^{1/3}, M \simeq |\dot{M}|t. \quad \text{(B14)}$$

B3 In the isothermal halo approximation

In an isothermal halo with constant circular velocity $V_{\rm c}$ the density within the Jacobi radius depends on $R_{\rm G}$ as

$$\rho_{\rm J} = \frac{3}{2\pi G}\frac{V_{\rm c}^2}{R_{\rm G}^2}, \quad \text{(B15)}$$

$$\simeq 5.376\left(\frac{R_{\rm G}}{\rm kpc}\right)^{-2}. \quad \text{(B16)}$$

In the last step we used $V_{\rm c} = 220\,{\rm km\,s^{-1}}$. If we use the constants as described in Section 2: $(r_{\rm h}/r_{\rm J})_1 = 0.145$, $\zeta = 0.2$ and $G \simeq 4.5\times10^{-3}\,{\rm pc^3\,M_\odot^{-1}\,Myr^{-2}}$ then from equation (B2) we obtain

$$|\dot{M}| \simeq 20\,{\rm M_\odot\,Myr^{-1}}\left(\frac{\rm R_G}{\rm kpc}\right)^{-1}. \quad \text{(B17)}$$

The tracks and isochrones for $\rho_{\rm h}$ are shown in Section 3 using this isothermal halo approximation. For the isochrones an age of 13 Gyr was used.

APPENDIX C: TRACKS AND ISOCHRONES IN UNITS OF M, $\rho_{\rm h}$ AND $R_{\rm G}$, INCLUDING THE ESCAPE TIME EFFECT

If we include the effect of the escape time (Appendix A) we get for the mass evolution

$$M(M_0,t) = \left(M_0^x - \hat{M}_x t\right)^{1/x}, \quad \text{(C1)}$$

where

$$\hat{M}_x \simeq 35.4\zeta\left(\frac{G\rho_{\rm J}}{[r_{\rm h}/r_{\rm J}]_1^3}\right)^{1/2}\frac{x}{M_1^{1-x}}. \quad \text{(C2)}$$

Here $M_1 \equiv \bar{m}N_1$ is a constant reference mass that has a similar role as N_1 introduced in Appendix A, and we again adopt $\bar{m} = 0.5{\rm M_\odot}$. Note that $\hat{M}_x$ is not anymore the time-derivative of M.

C1 Tracks

Using equation (16) for $\tau_{\rm cr1}$, we find that the tracks for general x are

$$\rho_{\rm h}(\rho_{\rm J},M_0,t) = \frac{A^2}{2}\left(\frac{r_{\rm h}}{r_{\rm J}}\right)_1^{-3}\rho_{\rm J}\left(\frac{M_0}{M_1}\right)^{2-2x}\left(1-\frac{\hat{M}_x t}{M_0^x}\right)^{2/x-2} \times\left(1-\left[1-\frac{\hat{M}_x t}{M_0^x}\right]^{(7/2)/x-1}\right)^{-2}, \quad \text{(C3)}$$

$$\rho_{\rm h}(M_0,t) \simeq \frac{1}{G}\left(\frac{M_0}{125\zeta t}\right)^2, \quad M_0^x \gg \hat{M}_x t, \quad \text{(C4)}$$

$$\rho_{\rm h}(\rho_{\rm J},M_0,t) \simeq \frac{A^2}{2}\left(\frac{r_{\rm h}}{r_{\rm J}}\right)_1^{-3}\rho_{\rm J}\left(\frac{M_0}{M_1}\right)^{2-2x} \times\left(1-\frac{\hat{M}_x t}{M_0^x}\right)^{2/x-2}, \quad M_0^x \simeq \hat{M}_x t, \quad \text{(C5)}$$

or in terms of radius

$$r_{\rm h}(\rho_{\rm J},M_0,t) = \left(\frac{6}{8\pi A^2}\right)^{1/3}\left(\frac{r_{\rm h}}{r_{\rm J}}\right)_1\left(\frac{M_0}{\rho_{\rm J}}\right)^{1/3}\left(\frac{M_0}{M_1}\right)^{(2x-2)/3} \times\left(1-\frac{\hat{M}_x t}{M_0^x}\right)^{(2-1/x)/3}\left(1-\left[1-\frac{\hat{M}_x t}{M_0^x}\right]^{(7/2)/x-1}\right)^{2/3}, \quad \text{(C6)}$$

$$r_{\rm h}(M_0,t) \simeq \left(\frac{3G}{8\pi M_0}\right)^{1/3}(125\zeta t)^{2/3}, \quad M_0^x \gg \hat{M}_x t, \quad \text{(C7)}$$

$$r_{\rm h}(\rho_{\rm J},M_0,t) \simeq \left(\frac{6}{8\pi A^2}\right)^{1/3}\left(\frac{r_{\rm h}}{r_{\rm J}}\right)_1\left(\frac{M_0}{\rho_{\rm J}}\right)^{1/3}\left(\frac{M_0}{M_1}\right)^{(2x-2)/3} \times\left(1-\frac{\hat{M}_x t}{M_0^x}\right)^{(2-1/x)/3}, \quad M_0^x \simeq \hat{M}_x t. \quad \text{(C8)}$$

C2 Isochrones

The isochrones for variable x can be found from the tracks by insertion of an expression for $M_0(M,\hat{M}_x,t)$ (equation C1)

$$\rho_{\rm h}(\rho_{\rm J},M,t) = \frac{A^2}{2}\left(\frac{r_{\rm h}}{r_{\rm J}}\right)_1^{-3}\rho_{\rm J}\left(\frac{M}{M_1}\right)^{2-2x} \times\left(1-\left[1+\frac{\hat{M}_x t}{M^x}\right]^{1-(7/2)/x}\right)^{-2}, \quad \text{(C9)}$$

$$\rho_{\rm h}(M,t) \simeq \frac{1}{G}\left(\frac{M}{125\zeta t}\right)^2,\ M^x \gg \hat{M}_x t, \quad \text{(C10)}$$

$$\rho_{\rm h}(\rho_{\rm J},M) \simeq \frac{A^2}{2}\left(\frac{r_{\rm h}}{r_{\rm J}}\right)_1^{-3}\rho_{\rm J}\left(\frac{M}{M_1}\right)^{2-2x},\ M^x \simeq \hat{M}_x t, \quad \text{(C11)}$$

or in terms of radius

$$r_{\rm h}(\rho_{\rm J},M,t) = \left(\frac{6}{8\pi A^2}\right)^{1/3}\left(\frac{r_{\rm h}}{r_{\rm J}}\right)_1\left(\frac{M}{\rho_{\rm J}}\right)^{1/3}\left(\frac{M}{M_1}\right)^{(2x-2)/3} \times\left(1-\left[1+\frac{\hat{M}_x t}{M^x}\right]^{1-(7/2)/x}\right)^{2/3}, \quad \text{(C12)}$$

$$r_{\rm h}(M,t) \simeq \left(\frac{3G}{8\pi M}\right)^{1/3}(125\zeta t)^{2/3},\ M^x \gg \hat{M}_x t, \quad \text{(C13)}$$

$$r_{\rm h}(\rho_{\rm J},M) \simeq \left(\frac{6}{8\pi A^2}\right)^{1/3}\left(\frac{r_{\rm h}}{r_{\rm J}}\right)_1\left(\frac{M}{\rho_{\rm J}}\right)^{1/3} \times\left(\frac{M}{M_1}\right)^{(2x-2)/3},\ M^x \simeq \hat{M}_x t. \quad \text{(C14)}$$

C3 Implications for the comparison to Milky Way globular clusters

The main change that follows from the introduction of $x \neq 1$ occurs in the evaporation dominated phase where we do not have a constant $r_{\rm h}/r_{\rm J}$ anymore, but instead

$$\rho_{\rm h}/\rho_{\rm J} \propto M^{2-2x}, \quad \text{(C15)}$$

or

$$r_{\rm h}/r_{\rm J} \propto M^{2(x-1)/3}. \quad \text{(C16)}$$

For $x = 3/4$ and the isothermal halo approximation these scaling relations are equivalent to

$$\rho_{\rm h} \propto M^{1/2}R_{\rm G}^{-2}, \quad \text{(C17)}$$

or

$$r_{\rm h} \propto M^{1/6}R_{\rm G}^{2/3}. \quad \text{(C18)}$$

So at a given $R_{\rm G}$ this relation implies that $r_{\rm h} \propto M^{1/6}$, depending on the exact value of x[4]. If we would have taken the Coulomb logarithm into account, the index of $1/6$ would be slightly smaller. So the particular scaling of $\tau_{\rm esc} \propto \tau_{\rm rh}^{3/4}$ has as a result that in the regime where mass loss dominates the cluster half-mass radius is (nearly) independent of M and is determined mainly by the tidal field strength. In the expansion dominated phase we still find $\tau_{\rm cr} \propto N^{-1}$, or $\rho_{\rm h} \propto M^2$, at a given age.

[4] A relation $r_{\rm h} \propto M^0$ is found for $x = 1/2$.